SLAC–PUB–4816
February 1989
(T/E)

Z° PHYSICS AT THE SLC*

JONATHAN M. DORFAN
Stanford Linear Accelerator Center
Stanford University, Stanford, CA 94309

TABLE OF CONTENTS

* Work supported by the Department of Energy, DE–AC03–7600515.

Invited Lectures given at the Banff Summer Institute on Particles and Fields, Banff, Canada, August 14–27, 1988, and the Nato Advanced Study Institute on the Techniques and Concepts of High Energy Physics, St. Croix, U.S. Virgin Islands, July 14–25, 1988,

1. ABSTRACT

This report summarizes the material covered in two lectures given during the summer of 1988. The same two lectures were given at both the Banff Summer Institute and the Advanced Study Institute on Techniques and Concepts of High Energy Physics at St. Croix. In both cases the audience was a mixture of recent and soon-to-be Ph.D.'s. The original intent of these lectures was to discuss the early physics results from the MARKII program at the SLC. Given the delayed start of this program, the focus of the lectures was changed to discuss the detailed studies which have been carried out on how to extract the physics. To put the discussion of the measurements in context, a brief summary of the Standard Model is presented along with a discussion of the MARKII detector and the energy measurement spectrometers. In areas where there has been little or no change from previous write-ups which I have done,[1] I have lifted the text from these write-ups. However, where the techniques have improved, this report reflects those changes.

2. INTRODUCTION

The discovery at CERN[2] of the Z° in $\bar{p}p$ collisions was a spectacular achievement. Background-free signals in both the $Z^\circ \to e^+e^-$ and $Z^\circ \to \mu^+\mu^-$ channels were seen which provided the first direct observation of the neutral weak force carrier. However, because of the difficulties inherent in the $\bar{p}p$ environment, detailed studies of the decays of the Z°, and hence, detailed studies of the weak interaction, were not possible. The main difficulties are two-fold (refer to Fig. 1):

1. Z° production is a small part of the total $\bar{p}p$ collision cross section. There is no way to "tune" the hard collision, constituent subenergy $\hat{s}$, to the Z° mass. Rather one is at the mercy of the overlap of the distribution functions of the two partons to conspire to provide $\hat{s} = M_Z^2$.

2. Once a Z° is produced it must be detected in the presence of the large hadronic debris which results from the partons which did not participate in the hard collision. The only practical method for beating down these large backgrounds is to tag the Z° using its leptonic decay modes. This has the disadvantage of a small yield ($BF(Z^\circ \to e^+e^-, \mu^+\mu^- = 3\%)$ and does not permit an unbiased and systematic study of all the decay modes of the Z°.

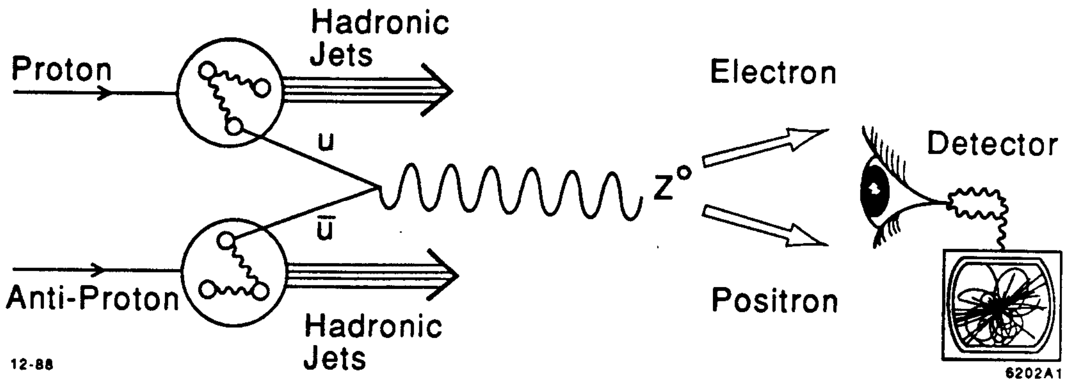

Fig. 1. A pictorial view of $\bar{p}p$ collision in which a u quark from the proton and a $\bar{u}$ quark from the anti-proton combine to form a Z°. The remaining partons produce debris in the form of hadronic jets. The Z° is envisaged to decay to an electron-positron pair which will be distinctive enough to unravel them from the hadrons, thereby forming a tag for the Z°.

The collider results provide us with a relatively crude measurement of the Z° mass:

$$M_{Z^\circ} = 91.5 \pm 1.2 \pm 1.7 \ \text{GeV/c}^2 \quad \text{(UA2)} \quad ,$$

$$M_{Z^\circ} = 93.1 \pm 1.0 \pm 3.1 \ \text{GeV/c}^2 \quad \text{(UA1)} \quad .$$

This measurement is systematics limited, the major problem being the lack of precise knowledge of the calorimeter energy scale (the measurement comes from the $Z^\circ \rightarrow e^+e^-$ mode).

The next major step in improving our understanding of the Z° will come from studies at the SLC and LEP which will provide a background-free data set of Z° produced via e^+e^- collisions. This environment overcomes the problems of the $\bar{p}p$ colliders; one is able to tune the collision energy precisely to the $Z^\circ(\hat{s} \equiv s), Z^\circ$ particle production totally dominates all other processes and Z°'s can be studied in an unbiased, debris-free environment.

3. THE STANDARD MODEL AND ITS APPLICATION TO $e^+e^- \rightarrow Z^\circ \rightarrow f\bar{f}$

For most of these lectures we will assume the Standard Model. When we look beyond the Standard Model, we will develop whatever formalism we need. The goal of this Section is not to be complete or detailed—but merely to build a foundation from which we can extract useful experimental tests at the Z°.

The Standard Model is characterized by the gauge group

$$\mathrm{SU}(3)_{color} \wedge \mathrm{SU}(2) \wedge \mathrm{U}(1).$$

Leptons are pointlike particles which couple to the gauge bosons of SU(2) through their weak charge and to the photon of U(1) through their electric charge. There are six leptons e, μ, τ, and their zero mass partners ν_e, ν_μ, and ν_τ. There are six quarks u, d, s, c, b and t which carry color and there are three color states for each quark. Leptons have no color charge and are therefore "blind to the strong interaction.

The left-handed fermions are arranged in weak iso-doublets

$$\begin{pmatrix} \nu_e \\ e \end{pmatrix}_L \quad \begin{pmatrix} \nu_\mu \\ \mu \end{pmatrix}_L \quad \begin{pmatrix} \nu_\tau \\ \tau \end{pmatrix}_L \qquad \begin{matrix} T_3 = 1/2 \\ 1/2 \end{matrix} \quad ,$$

$$\begin{pmatrix} u \\ d' \end{pmatrix}_L \quad \begin{pmatrix} c \\ s' \end{pmatrix}_L \quad \begin{pmatrix} t \\ b' \end{pmatrix}_L \qquad \begin{matrix} T_3 = 1/2 \\ -1/2 \end{matrix} \quad ,$$

where T_3 is the 3rd component of the weak charge. The primes on the quarks indicate that flavor conservation in the quark sector is not perfect. This generation mixing can be summarized by the elements of the Kobayashi–Maskawa matrix—the most familiar component being the Cabibbo angle which tells us that the d quark has $\sim 5\%$ strange quark admixture. More succinctly, in the quark sector the weak eigenstates are related by a rotation matrix to the mass eigenstates. We notice in passing, the peculiarity of the three generations; the ν_e, e, u and d being the members of the lightest generation. The Standard Model does not explain why nature chooses to replicate itself in this peculiar manner.

Right-handed fermions appear in singlets, u_R, d_R $\ldots t_R$, e_R, μ_R, τ_R and, since the ν's are massless, there are no right-handed ν's. $T_3 = 0$ for all right-handed fermions.

There are nine massless bosons in the Standard Model—eight gluons and the photon. There are three massive vector bosons W^+, W^- and Z^0 and, in the minimal model with one Higgs doublet, there is one neutral scalar, H^0. Gluons carry color (unlike photons which don't carry charge) and hence $SU(3)_{color}$ is non–Abelian. Since gluons carry color, they can couple to other gluons. The polarization of the QCD vacuum by virtual quark and gluon pairs results in an *anti-screening* of color charge. This can be contrasted with the *screening* of electric charge by virtual e^+e^- pairs in QED. This anti-screening leads to the notion of confinement of quarks and the decrease of the strong coupling constant, α_s, with increasing q^2. Free quarks should not be seen, and this notion will be tested at the Z^0 although not discussed further in these lectures.

The Standard Model does not predict masses for the fundamental particles. The $W^\pm$, Z^0 masses, ignoring electroweak radiative effects, are given in terms of the parameter $\sin^2\theta_w$:

$$M_W^2 = \frac{\pi\alpha}{\sqrt{2}G_F}\left(\frac{1}{\sin^2\theta_w}\right)$$

$$M_{Z^0}^2 = \frac{M_W^2}{\cos^2\theta_w} = \frac{\pi\alpha}{\sqrt{2}G_F}\left(\frac{1}{\sin^2\theta_w\cos^2\theta_w}\right) \quad ,$$

where α is the fine structure constant and G_F is the Fermi coupling constant. The H^0 mass is expected to fall in the range $7.5 \lesssim M_{H^0} \lesssim 10^3$ GeV. This, however, is of no consolation to the experimentalist searching for the H^0. The presence of the neutral Higgs is crucial to the success of the Standard Model.

There is nothing fundamental about the minimal Higgs scheme. The model is constrained by the measured value of $\rho = 1$ to contain explicitly doublets (as opposed to triplets). A non-minimal model with two doublets (eight fields) is perfectly acceptable. In this case, three of the fields are needed to provide mass for the $W^\pm$ and Z^o leaving five physical Higgs particles. These are two neutral scalars, H_1^o and H_2^o; one pseudoscalar h^o (often called an axion); and two charged pseudoscalars H^+ and H^-. In such a model, the lower mass limit of 7.5 GeV/c^2 no longer pertains.

The electroweak interactions of all the gauge fields are specified by the model and are determined by e, the electric charge, and one free parameter θ_w. Spinors couple to the photon field with strength e and to the Z^0 with strength

$$-\frac{e}{\sin\theta_w\cos\theta_w}\left(T_3^{R/L} - Q\sin^2\theta_w\right) = 2\sqrt{2}\left(\frac{M_Z^2G_F}{\sqrt{2}}\right)^{1/2}\left(T_3^{R/L} - Q\sin^2\theta_w\right)$$

where R/L indicates left and right couplings and Q is the charge of the fermion.

Aside from Higgs and fermion masses, the Electroweak theory is totally specified if we know α, G_F and M_Z; α and G_F are extremely accurately known (better than one part in 10^5), whereas M_Z is known only to about 2%. A precise measurement of M_Z will constrain considerably the Standard Model.

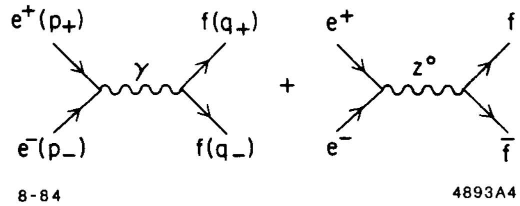

Fig. 2. The basic $e^+e^- \to \gamma,\ Z^\circ$ process.

For almost all the physics discussed in these lectures, we are interested in the basic process $e^+e^- \to f\bar{f}$ where the symbol f signifies a fundamental fermion, either a quark or a lepton. There are two processes which contribute to the cross section as shown in Fig. 2, namely $e^+e^- \to \gamma \to f\bar{f}$ and $e^+e^- \to Z^0 \to f\bar{f}$. The Standard Model specifies all the couplings and hence the cross section for these processes can be calculated. If θ is the fermion polar angle, the differential cross section has the form[3]

$$
\begin{aligned}
\frac{d\sigma_{f\bar{f}}}{d\cos\theta} = {} & \frac{\pi\alpha^2 Q_f^2 D}{2s}\,(1+\cos^2\theta) - \frac{\alpha Q_f D G_F M_z^2(s-M_z^2)}{8\sqrt{2}[(s-M_z^2)^2+M_z^2\Gamma_z^2]} \\
& \left[(R_e+L_e)(R_f+L_f)(1+\cos^2\theta)+2(R_e-L_e)(R_f-L_f)\cos\theta\right] \\
& + \frac{D G_F^2 M_z^4 s}{64\pi[(s-M_z^2)^2+M_z^2\Gamma_z^2]} \\
& \left[(R_e^2+L_e^2)(R_f^2+L_f^2)(1+\cos^2\theta)+2(R_e^2-L_e^2)(R_f^2-L_f^2)\cos\theta\right] \quad ,
\end{aligned}
\tag{1}
$$

where Q_f is the fermion charge, $s = E^2_{c.m.}$, M_Z the mass of the Z^0 and D takes into account the number of color degrees of freedom. For $f \equiv$ quark, $D = 3$; otherwise $D = 1$. The left- and right-handed weak coupling constants are given by

$$L_f = T_3^f - Q_f \sin^2\theta_w$$

$$R_f = -Q_f \sin^2\theta_w \quad .$$

The three terms in the cross section are the purely electromagnetic contribution, the interference between the weak and electromagnetic diagrams and the purely weak contribution. Notice that (a) the interference term disappears at $\sqrt{s} = M_Z$ as it should (b) the first term is just the point QED differential cross section and (c) at $\sqrt{s} = M_Z$, the purely weak term dominates.

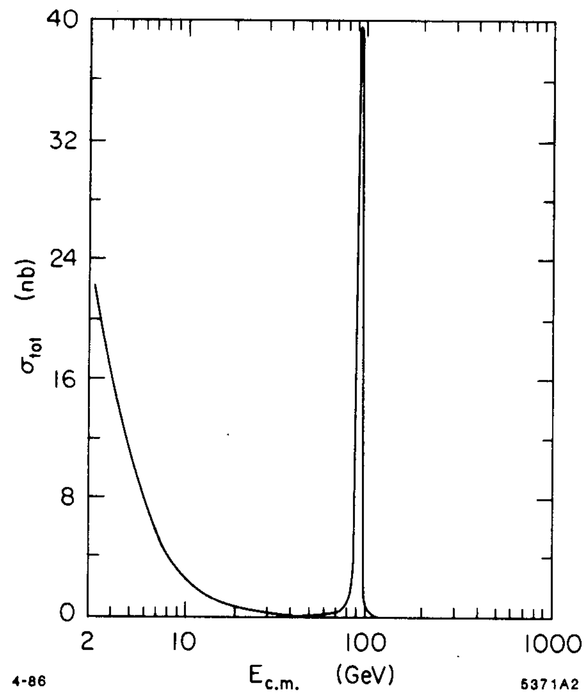

Fig. 3. The cross section for $e^+e^- \to \gamma,\ Z^\circ \to f\bar{f}$ as calculated in the Standard Model. The $c\bar{c}$ and $b\bar{b}$ threshold behavior are omitted from the plot.

It is illustrative to integrate over $\cos\theta$ and plot the cross section as a function of $E_{c.m.} = \sqrt{s}$. This is shown in Fig. 3 for hadronic final states. One sees that below the region of the Z^0 mass, the purely electromagnetic cross section dominates as is reflected by the $E_{c.m.}^{-2}$ behavior. On the Z° pole however the weak cross section dominates, providing 10^3 times more particle production than the electromagnetic process. This is part of the magic of running at the Z^0—the Z° provides an enormous enhancement in event rate over running in the continuum (*i.e.*, off resonance). Studying e^+e^- interactions at $\sim$ 92 GeV in the absence of the Z° with the SLC or LEP would be ex- tremely painful if not in many cases impossible. The presence of the Z°, however, renders these relatively low luminosity machines capable of very high event rates.

Let us now return to $d\sigma/d\cos\theta$ and consider running at $s = M_Z^2$, namely on the Z° pole. Changing notation to axial and vector coupling constants

$$a = \frac{1}{2}(L - R) \quad \text{and} \quad v = \frac{1}{2}(L + R) \quad ,$$

one finds $L = a + v$, $R = v - a$, $L^2 + R^2 = 2(a^2 + v^2)$, $L^2 - R^2 = 4av$ and

$$\frac{d\sigma_{f\bar{f}}}{d\cos\theta} = \frac{DG_F^2 M_Z^4}{16\pi\Gamma_Z^2}\left[(a_e^2 + v_e^2)(a_f^2 + v_f^2)(1 + \cos^2\theta) + 8a_e v_e a_f v_f \cos\theta\right] \quad . \tag{2}$$

It is useful to tabulate the couplings and the sum of their squares. Assuming $\sin^2\theta_W = 0.23$ (which we will do throughout for convenience) we find the values in Table I.

Table I

	Q	T_3	a	v	$a^2 + v^2$
e, μ, τ	-1	$-1/2$	$-1/2$	$-.04$	.2516
ν_e, ν_μ, ν_τ	0	1/2	1/2	1/2	1/2
d, s, b	$-1/3$	$-1/2$	$-1/2$	$-.347$	.370
u, c, t	$+2/3$	$+1/2$	1/2	.193	.287

We turn our attention back to Eq. (2). The term linear in $\cos\theta$ contributes a front–back asymmetry, A_{F-B}. $A_{F-B} \propto v_e v_f$ which, for charged leptons, is a very small number. However, a measurement of A_{F-B} for charged leptons has great sensitivity to $\sin^2\theta_w$ as we will see later in this section. Since $\int_0^\pi \cos\theta d\theta = 0$, the term linear in $\cos\theta$ does not contribute to the total cross section.

Integrating the term in $(1+\cos^2\theta)$ yields the total cross section for producing a final state $f\bar{f}$ at the Z^0 :

$$\sigma_{f\bar{f}} = \frac{DG_F^2 M_Z^4}{6\pi\Gamma_Z^2}\,(v_e^2+a_e^2)(v_f^2+a_f^2) \quad .$$

We omit here the derivation of Γ_Z, but note that

$$\Gamma_Z = \frac{G_F M_Z^3}{24\sqrt{2}\pi}\,\sum_i (v_i^2+a_i^2)D_i \quad , \tag{3}$$

where i ranges over all fundamental fermions and D_i is the color factor (three for quarks, one for leptons). We can obtain $\sigma_{\rm point}$, which is the lepton point QED cross section, from the first term in Eq. (1):

$$\begin{aligned}\sigma_{\rm point} &= \frac{\pi\alpha^2}{2s}\int(1+\cos^2\theta)\;d\cos\theta \\ &= \frac{4\pi\alpha^2}{3s} \simeq \frac{87\ \text{nb}}{s} \quad .\end{aligned}$$

Hence, we can write

$$R_{f\bar{f}} = \frac{\sigma_{f\bar{f}}}{\sigma_{\rm point}} = \frac{D(a_f^2+v_f^2)(a_e^2+v_e^2)}{16\alpha^2(1-2x_w+8x_w^2/3)^2} \quad . \tag{4}$$

where $x_w = \sin^2\theta_w$.

Assuming five quarks and $x_w = 0.23$, we find the total cross section

$$\begin{aligned}\sigma_{tot} = \sum_f \sigma_{f\bar{f}} &= \frac{DG_F^2 M_Z^4}{6\pi\Gamma_Z^2}(v_e^2+a_e^2)\sum_f(v_f^2+a_f^2) \\ &= 47\ \ nb\ \ \text{(no radiative corrections)} \\ &= 37\ \ nb\ \ \text{(with radiative corrections)}.\end{aligned}$$

Table II shows the R values (not radiatively corrected) and the branching fraction for each process. We notice that the Z° decays predominantly to hadrons

Table II

CHANNEL ($f\bar{f}$)	$R_{f\bar{f}}$	$\Gamma_{f\bar{f}}/\Gamma_{Z^\circ}$ (%)
each $\nu\bar{\nu}$	319	6.1
$\mu^+\mu^-$, $\tau^+\tau^-$, e^+e^{-*}	160	3.1
$u\bar{u}$, $c\bar{c}$, $t\bar{t}$	550	10.6
$d\bar{d}$, $s\bar{s}$, $b\bar{b}$	709	13.6

* We have ignored t channel diagrams which are only important at small values of θ.

($BF(Z^\circ \rightarrow hadrons) = 72\%$), and that the weak interaction (modulo the color factor) is rather democratic. One therefore produces roughly equal amounts of $Z^\circ \rightarrow b\bar{b}$ and $Z^\circ \rightarrow c\bar{c}$, in contrast to the electromagnetic interaction where quark production rates go like the electric charges squared and, hence, one gets four times as much $c\bar{c}$ production as $b\bar{b}$ production.

The physics at the Z° cannot be extracted without paying careful attention to the effects of radiative corrections. In lowest order, the Z° line shape is a Breit–Wigner which is characterized by three parameters: mass, width and peak cross section. Radiative corrections, and most notably initial state $e^\pm$ Bremsstrahlung, will alter these quantities significantly. A complete treatment of this subject goes way beyond these lectures, but is covered very clearly and thoroughly in Ref. 4. Here we will simply indicate the results as they effect the measurements and comment that, due to the considerable effort of the past few years (as summarized in Ref. 4), no measurements will be limited in precision by our present understanding of the radiative corrections. Other measurement errors will always dominate.

In the absence of a resonance, initial state Bremsstrahlung in e^+e^- collisions lowers the effective collision energy, which raises the cross section ($\sigma_{e^+e^-} \sim E_{cm}^{-2}$). Given a giant resonance like the Z°, one must convolute the Bremsstrahlung spectrum with the resonance line shape, altering significantly the resonance parameters. As discussed in Ref. 4 there are two classes of corrections to consider —

electroweak and QCD. These are shown schematically in Fig. 4. QCD corrections occur, of course, only in final states involving hadronic production.

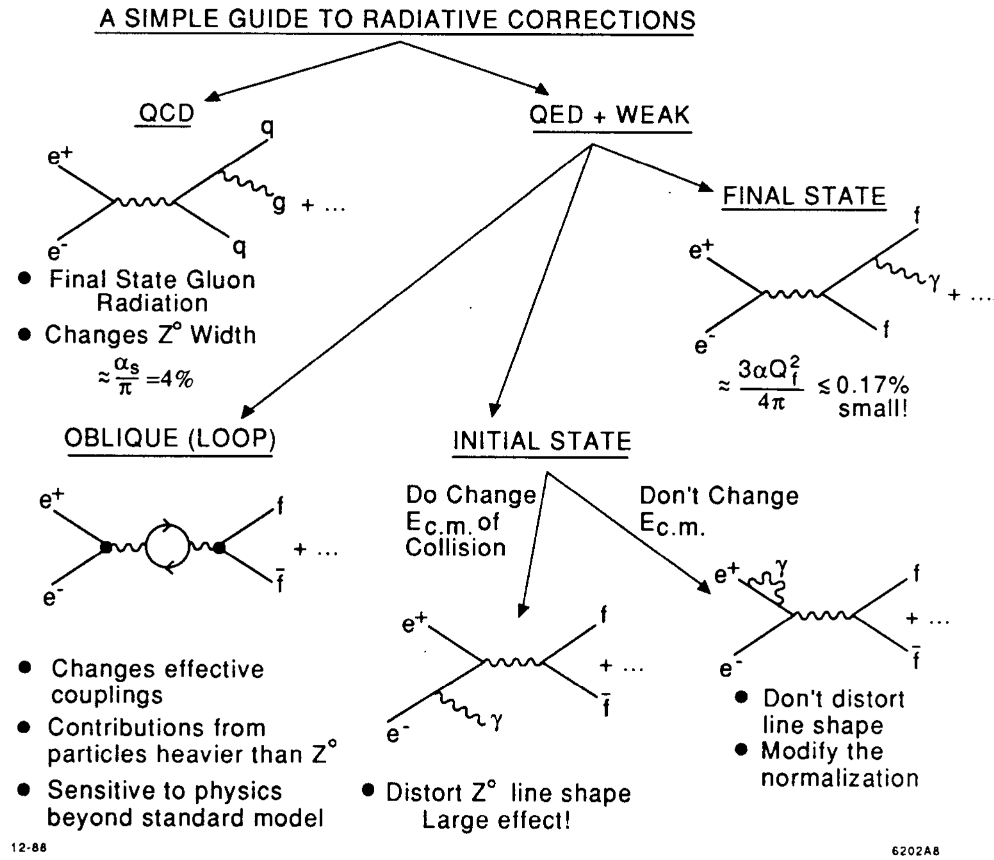

Fig. 4. A diagramatic guide to radiative corrections to $e^+e^- \to Z^\circ \to f\bar{f}$.

They are proportional to $\alpha_s/\pi \approx 4\%$ and directly effect the Z° width. Final state electromagnetic corrections are at the level of $3\alpha Q_f^2/4\pi < 0.17$ and can safely be ignored. Oblique corrections (see Fig. 4) contain internal loops of leptons and bosons and have the effect of changing the effective couplings. They can involve particles in the loops which are heavier than the Z°, and hence have sensitivity, in principle, to physics beyond the Standard Model. Initial state electromagnetic radiation can occur without a change in collision energy via vertex correction diagrams which do not distort the line shape but modify the overall normalization. Finally, there are the initial state Bremsstrahlung corrections which are by far the largest effect. They do change the collision energy and hence distort the Z° line shape in a substantial way. As discussed above and extensively in Ref. 4, the effects of the initial state QED radiation are now very well understood. The two second-order calculations available and the exponentiated first-order calculation agree remarkably well. Generators incorporating this theoretical input are also available for understanding the effects of detector inadequacies. Figure 5 shows the $Z^\circ \to \mu^+\mu^-$ cross section (M_z = 93 GeV/c^2) for four different calculations. One sees clearly that first-order would be insufficient, but the agreement between the two second-order and the exponentiated first-order are excellent. So, while the radiative effects shift the observed mass up by about 100 MeV/c^2 and raise Γ_z by about 3%, these shifts are now believed to be understood at a level of <10 MeV. The intrinsic experimental errors in measuring these quantities are more like 30 MeV; hence the statement that the precision of the Z° mass and width measurements will not be subject to the present accuracy of the effects of radiative corrections.

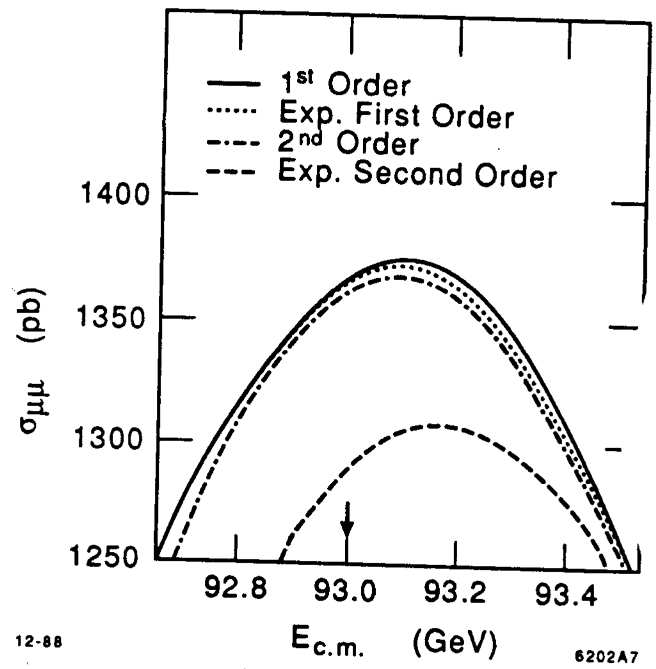

Fig. 5. The effect of electroweak radiative corrections on the $Z^\circ \to \mu^+\mu^-$ cross section. Four different calculations are shown as indicated by the figure key.

Returning then to the predictions of the Standard Model, Γ_z is given by

$$\Gamma_z = \frac{G_F M_Z^3}{24\sqrt{2}\pi} \sum_f D_f (v_f^2 + a_f^2)(1 + \delta_f) \quad ,$$

where δ_f = radiative corrections; $\delta_f = 3\alpha Q_f^2\, 4\pi$ for leptons, $= \alpha_{/}\pi$ for quarks. Hence for five quarks, $\sin^2\theta_w = 0.23$ and including the radiative corrections, the Standard Model predicts

$$\Gamma_z(5 \text{ quarks}) = 2.54 \quad \text{GeV} \quad .$$

If Γ_z is significantly larger than this value, there must exist physics beyond the Standard Model. The bench mark for measuring increases in the width is the contribution of one massless ν, namely

$$\Gamma(Z^\circ \to \nu\bar{\nu}) = 160 \quad \text{MeV} \quad .$$

Now, leptons or quarks produced at the Z° will necessarily be heavy given the limits from TRISTAN, PETRA and the $\bar{p}p$ collider at CERN. In this case—$m_f/M_z \approx 1$—we must take into account threshold effects. In a general way we can write

$$\frac{d\sigma_{f\bar{f}}}{d\theta} = f(\beta_f, \theta)\ \sigma(m_f = 0)$$

and

$$\sigma_{f\bar{f}} = f(\beta_f)\sigma(m_f = 0)$$

where β_f is the fermion velocity and m_f is the fermion mass. For *vector* couplings

$$f(\beta_f, \theta) = \frac{3}{16\pi}\ \beta_f[(1 + \cos^2\theta) + (1 - \beta_f^2)\sin^2\theta]$$

and

$$f(\beta_f) = \frac{1}{2}\ \beta_f(3 - \beta_f^2) \quad .$$

For *axial-vector* couplings

$$f(\beta_f, \theta) = \frac{3}{16\pi}\, \beta_f^3 (1 + \cos^2\theta)$$

and

$$f(\beta_f) = \beta_f^3 \quad .$$

Therefore, for the t quark with velocity β_t, the correct form of the contribution to the Z^0 width is [see Eq. (3)]

$$\Gamma(Z^0 \to t\bar{t}) = \frac{G_F M_Z^3}{8\sqrt{2}\pi} \left(v_t^2\, \frac{1}{2}\, \beta_t (3 - \beta_t^2) + a_t^2 \beta_t^3 \right) \ .$$

Figure 6 shows the suppression of $t\bar{t}$ relative to a full strength (light) charge two-thirds quark as a function of the t quark mass. Since we know from TRISTAN that $M_t \gtrsim 27.5$ GeV/c^2, the $t\bar{t}$ final state at the Z^0 is suppressed at least to 0.6 of the $u\bar{u}$ rate.

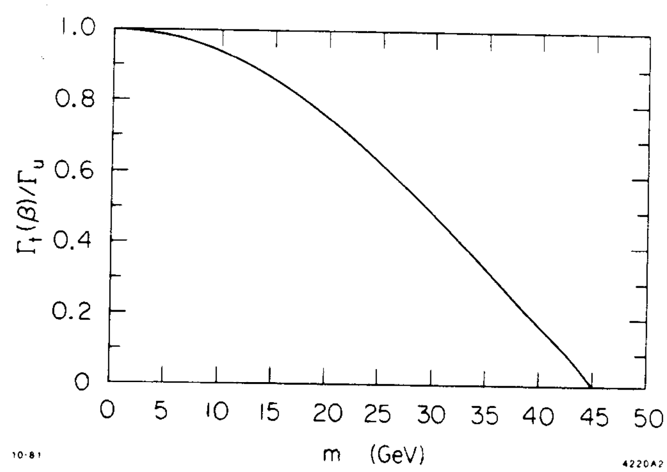

Fig. 6. The suppression factor of $t\bar{t}$ decays of the Z^0 as a function of M_t.

Because the weak interaction is parity violating, the reaction $Z^\circ \rightarrow f\bar{f}$ has a forward–backward charge asymmetry. The number of f's produced at θ do not equal the number of f's produced at $\pi - \theta$. From the master Eq. (2) we see this manifested in the terms linear in $\cos\theta$, which lead to the asymmetry:

$$A^f_{F-B} = \frac{\int_0^1 \frac{d\sigma}{dz}dz - \int_{-1}^0 \frac{d\sigma}{dz}dz}{\int_0^1 \frac{d\sigma}{dz}dz + \int_{-1}^0 \frac{d\sigma}{dz}dz} = \frac{N_f^F - N_f^B}{N_f^F + N_f^B} \quad ,$$

where $N_f^F(N_f^B)$ is the number of fermions in the forward (backward) hemisphere relative to the incoming e^- direction. On the Z^0 pole

$$A^f_{F-B} = \frac{3a_e v_e a_f v_f}{(a_f^2 + v_f^2)(a_e^2 + v_e^2)} \quad ,$$

which is quadratic in the vector coupling. Since the vector coupling for the leptons is small, A_{F-B} is a very small number for the charged leptons. For μ-pairs, which is experimentally a very attractive channel,

$$A^\mu_{F-B} = \frac{3(1 - 4\sin^2\theta_w)^2}{4(1 - 4\sin^2\theta_w + 8\sin^4\theta_w)^2}$$

$$= 1.9\% \;\; for \;\; \sin^2\theta_w = 0.23, \;\; 4.2\% \text{ for } \sin^2\theta_w = 0.22 \quad .$$

However, despite the smallness of A^μ_{F-B}, it has considerable sensitivity to $\sin^2\theta_w$, namely

$$\frac{d\sin^2\theta_w}{\sin^2\theta_w} = \frac{1}{23}\frac{dA^\mu_{F-B}}{A^\mu_{F-B}}.$$

Hence, large errors in A^μ_{F-B} are significantly beaten down by the large factor of 23. Quark asymmetries are much larger because $v_q >> v_\mu$: in particular for $Z^\circ \rightarrow b\bar{b}$,

$$A^b_{F-B} = 11\% \qquad \text{and} \qquad \frac{d\sin^2\theta_w}{\sin^2\theta_w} = \frac{1}{12}\frac{dA^b_{F-B}}{A^b_{F-B}} \quad .$$

An additional problem in measuring charge asymmetries is the rapid dependence of the asymmetry on the collision energy E_{cm}, as shown in Fig. 7 for $Z^\circ \rightarrow \mu^+\mu^-$

and $Z^\circ \to b\bar{b}$. Hence, intrinsic errors in E_{cm} (expected to be $\sim$ 30 MeV) contribute significantly to the error in A_{F-B}. For $Z^\circ \to \mu^+\mu^-, dA^\mu/dE_{cm} \approx 1\%/100$ MeV and for $Z^\circ \to b\bar{b}$, $dA^b/dE_{cm} \sim 0.2\%/100$ MeV. Again, the μ-pair channel is much more problematical than the $b\bar{b}$ final state.

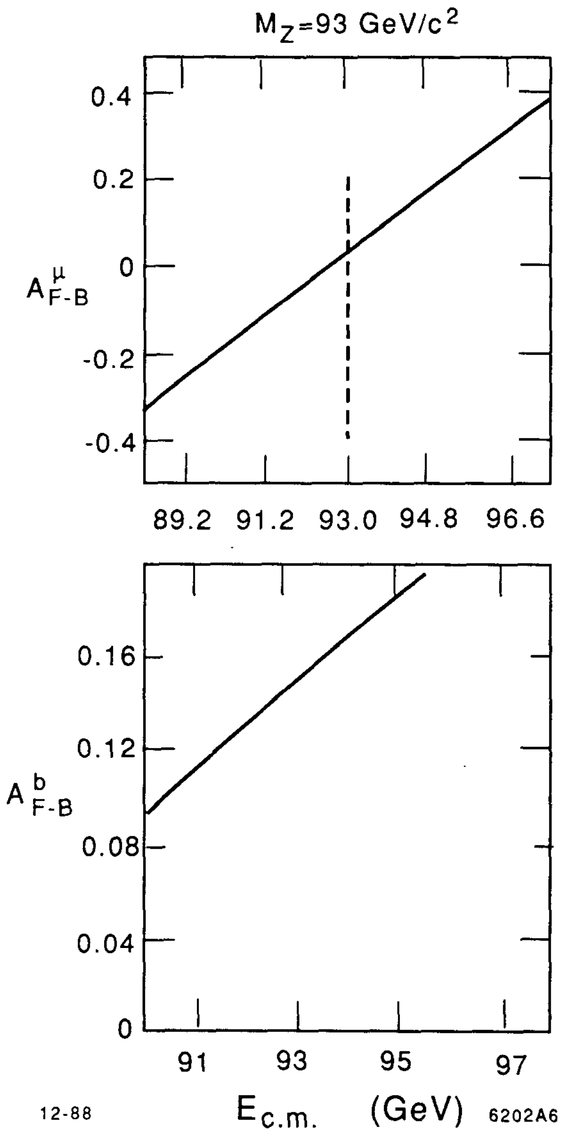

Fig. 7: The dependence of the foward backward asymmetry on E_{cm} and for $Z^\circ \to \mu^+\mu^-$ and $b\bar{b}$.

This, then, summarizes the theoretical predictions of the Standard Model. Figure 8 is a cartoon depiction of what Standard Model Z° decays will look like

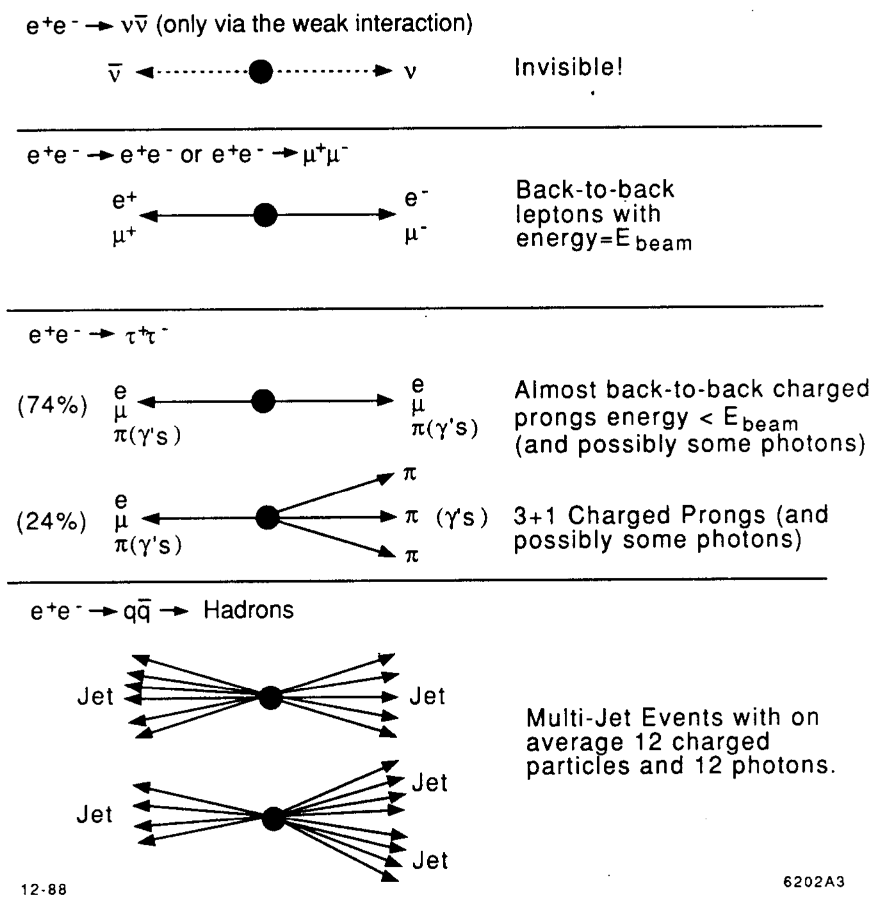

Fig. 8. A schematic representation of the primary expectations for Z° decays in the Standard Model.

in the detector. This will be the menu of *expected* events.

Despite its tremendous success, the Standard Model is sorely lacking as our ultimate theory. Presumably it is an excellent low energy approximation for the ultimate theory; few people believe that it will not be eclipsed.

There are many problems with the Standard Model. There are too many parameters (18), numbers which must be inserted by hand. It does not unify the forces, nor does it explain the pattern of masses or the presence of the generations. The Higgs mechanism is ad hoc and very unnatural, requiring exquisitely fine tuning to achieve its aim. These are but a few of the objections. It is most likely, that without further experimental clues, we will not make rapid progress in selecting the appropriate direction in which to depart from this model. Therefore, one of the major thrusts of the Z° studies will be to look for physics beyond the Standard Model. A large part of this write-up, then, is directed towards measurements which test the validity of the 3-generation Standard Model or which search for physics which is not directly contained in this model. The more pedestrian, but extremely rich, measurements which extend our knowledge of the presently known quarks and leptons are largely ignored. It should not escape the reader's attention that unprecedently large samples of quarks and leptons will be produced in Z° decays which will greatly enhance our knowledge about their properties.

As is well known, there do exist extensions and alternatives to the Standard Model. Typically, these models are aimed at a much more natural solution to the mass hierarchy problem. Supersymmetry (SUSY) and Technicolor are leading examples of such models, and it is entirely possible that these ideas are important pieces in the ultimate solution of the puzzle. These two models have a richer Higgs spectrum than the minimal Standard Model; both charged and neutral Higgs scalars must exist, if these ideas are correct. In addition, new constituents are predicted: sleptons and squarks for SUSY, technipions for Technicolor. With an increased particle spectrum then, these models are amenable to experimental verification.

What will be the role of the Z° in this quest for a better theoretical understanding?

1. We will be able to make much more precise tests of the electroweak sector of the Standard Model than are known today. Perhaps under such close scrutiny, chinks will begin to appear in the now formidable armor.
2. The top quark can be sought. While such a discovery would not violate anything in the Standard Model, a t quark mass as low as $M_z/2$ is getting very hard to accommodate in the parameter space of the 3-generation Standard

Model. Recent measurements, particularly $B\bar{B}$ mixing, tend to indicate a top mass >50 GeV/c^2 in a 3-generation model.

3. The generation problem can be confronted, either by direct searches for 4th generation charged fermions or by neutrino counting. Neutral heavy leptons are also easily found if they have masses below $M_Z/2$.
4. The Higgs sector can be studied both in the neutral and charged domain.
5. Searches for indications of physics beyond the Standard Model (SUSY or Technicolor objects) can be performed. Additional heavy bosons will show up as loop corrections to tree graphs and are accessible using polarized e^- beams.

To pin down the predictions of the electroweak sector, we need to know three parameters which can be chosen to be α, G_F and M_z. The first two are known to exquisite accuracy (<1 part in 10^7), but M_z is only known to about 2%. Fortunately this is measured with great precision (<35 MeV/c^2 at the SLC) with relatively few Z°'s and hence the model is immediately much more severely constrained. It is worth noting that while such a measurement sharpens markedly the predictions of the model, it does not constitute a test of the model. To do that requires an additional measurement as discussed later.

To illustrate how physics at the Z° will precede, I will restrict myself almost entirely to studies which have been made by the MARKII group who will be the first detector group to run at the SLC. These studies incorporate realistic detector simulations (raw data is produced) and real data analysis procedures. They should therefore represent realistic measures of the expected efficiencies and errors. The analyses discussed here are more thoroughly covered in Ref. 5(d). Clearly these studies have applicability to the LEP experiments and SLD (the MARKII replacement detector), although in most cases these detectors will bring more powerful tools to bear on the problem.

4. DETECTOR REQUIREMENTS; THE UPGRADED MARKII DETECTOR

The detector requirements must be well matched to the rigors of the environment. The Z° environment has been studied at great length and the interested reader can find summaries of these studies in Ref. 5. We mention here the essential elements as they pertain to the design of a Z° detector. Figure 9 summarizes the main spectrum of Z° decays which we are interested in studying, where the final state naming convention is given in the figure caption. We need to detect these final states efficiently and preserve the essential properties of the physics. We also need to monitor the integrated luminosity so that we can normalize the measurements. Precise measurement of the Z° mass and width require precise knowledge of the collision energy. For the SLC this is not provided by the machine and, hence, dedicated spectrometers had to be built. Characteristic decays of the unstable particles in Fig. 9 are given in Fig. 10. We notice that the environment is characterized by the presence of high energy jets, leptons, and missing energy. General detector requirements which follow then are:

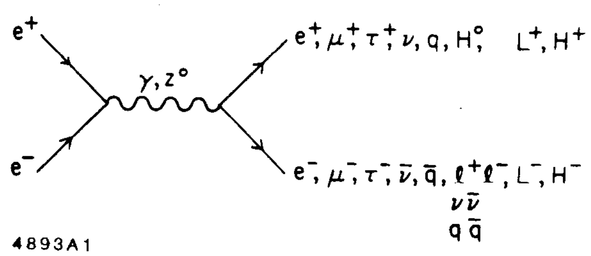

Fig. 9. The basic e^+e^- process where final states are produced via an intermediate photon or Z°. The notation is obvious except that q stands for a quark, H° the neutral Higgs scalar, $\ell^\pm$ a charged lepton, $H^\pm$ a charged Higgs scalar and $L^\pm$ a (new) heavy charged lepton.

1. The ability to measure the detailed properties of high multiplicity, high energy jets. These jets are typically comprised of 10 charged particles and 10 photons all contained within a cone of half angle 5°.

2. The ability to measure and identify electrons and muons over a wide range of momenta (1–50 GeV/c). These leptons must be tagged both in isolation and in the center of the dense jets.

3. The ability to measure as much of the collision energy as possible. Missing energy is a powerful tool for discovering new physics.

4. The ability to tag charm and bottom jets which is likewise important for the discovery and exploitation of new physics.

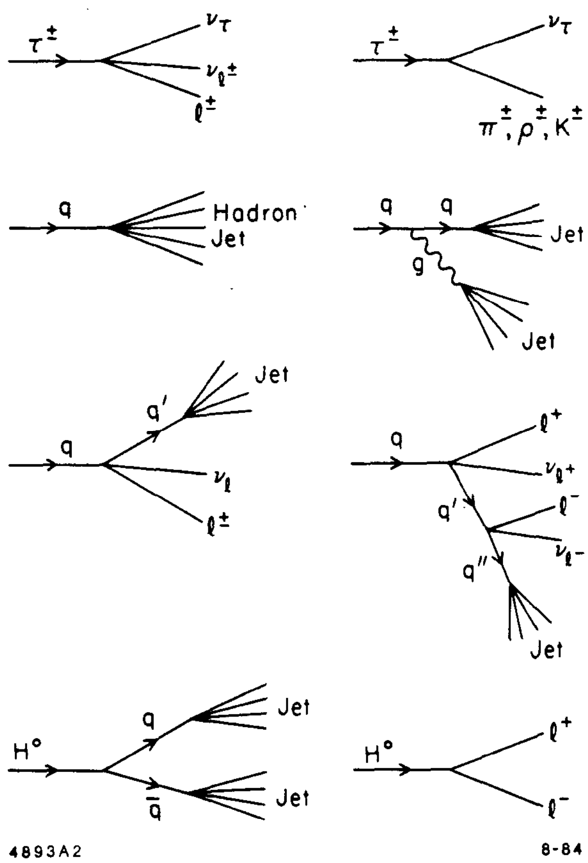

Fig. 10. Typical decays which result from the process in Fig. 9. The symbol g stands for a gluon.

In addition, there are many event topologies involving multiple jet and multiple leptons which demands that one instrument the detector uniformly over a large solid angle. To satisfy these demands requires large solid angle tracking with multihit capability, large solid angle calorimetry, good hermeticity down to small (≈50 mrad) angles relative to the beam axes, muon and electron coverage over a large solid angle with hadron rejection $> 10^3$ for momenta above 1 GeV/c and an excellent vertex detector placed at as small a radius as possible.

The MARKII detector was upgraded from its PEP configuration with an eye to satisfying as many of the above criteria as possible. The thrust of the MARKII program at the SLC was to begin with a well understood detector. The upgrades were made with sufficient haste so as to permit full checkout at PEP prior to installation at the SLC. Figure 11 shows an isometric view of the detector, Fig. 12 shows a cut through the transverse plane. The detector incorporates excellent tracking, hermetic calorimetry down to 15 mrads, excellent hadron/lepton separation and high resolution vertex detectors. It lacks hadron calorimetry and has no useful $\pi/K/p$ separation above 2 GeV/c.

Tracking is achieved with a 72-layer drift chamber in combination with a 5 kg magnetic field (non-cryogenic). The drift chamber has multihit electronics and a measured spatial resolution of 160 μm. The tracking system is fully efficient out to $cos\theta \simeq 0.85$ and drops to 50% around $cos\theta \simeq 0.9$. The intrinsic momentum resolution, incorporating the SLC vertex constraint, is $\sigma_p/p^2 = 0.2$, ignoring the effects of multiple scattering. Pulse height information is also available from the drift chamber, providing dE/dx information for electron identification with a resolution of 7.5%. Combining time-of-flight information with dE/dx provides excellent hadron rejection for momenta in the range 500 MeV/c to 5 GeV/c. Above 5 GeV/c, the calorimetry is used with comparable rejection. All three systems provide hadron rejection $> 10^3$ for momenta above 500 MeV/c.

The barrel plus endcap shower counters cover 95% of 4π and have an energy resolution of $13\%/\sqrt{E}$ and $20\%/\sqrt{E}$ (E in GeV), respectively. For high energy (>1GeV) isolated electrons they provide hadron rejection of $> 10^2$. The calorimeters have poorer rejection when the electrons are within a jet—in this case the power of the dE/dx systems is utilized. Figure 13 shows the calorimetry in

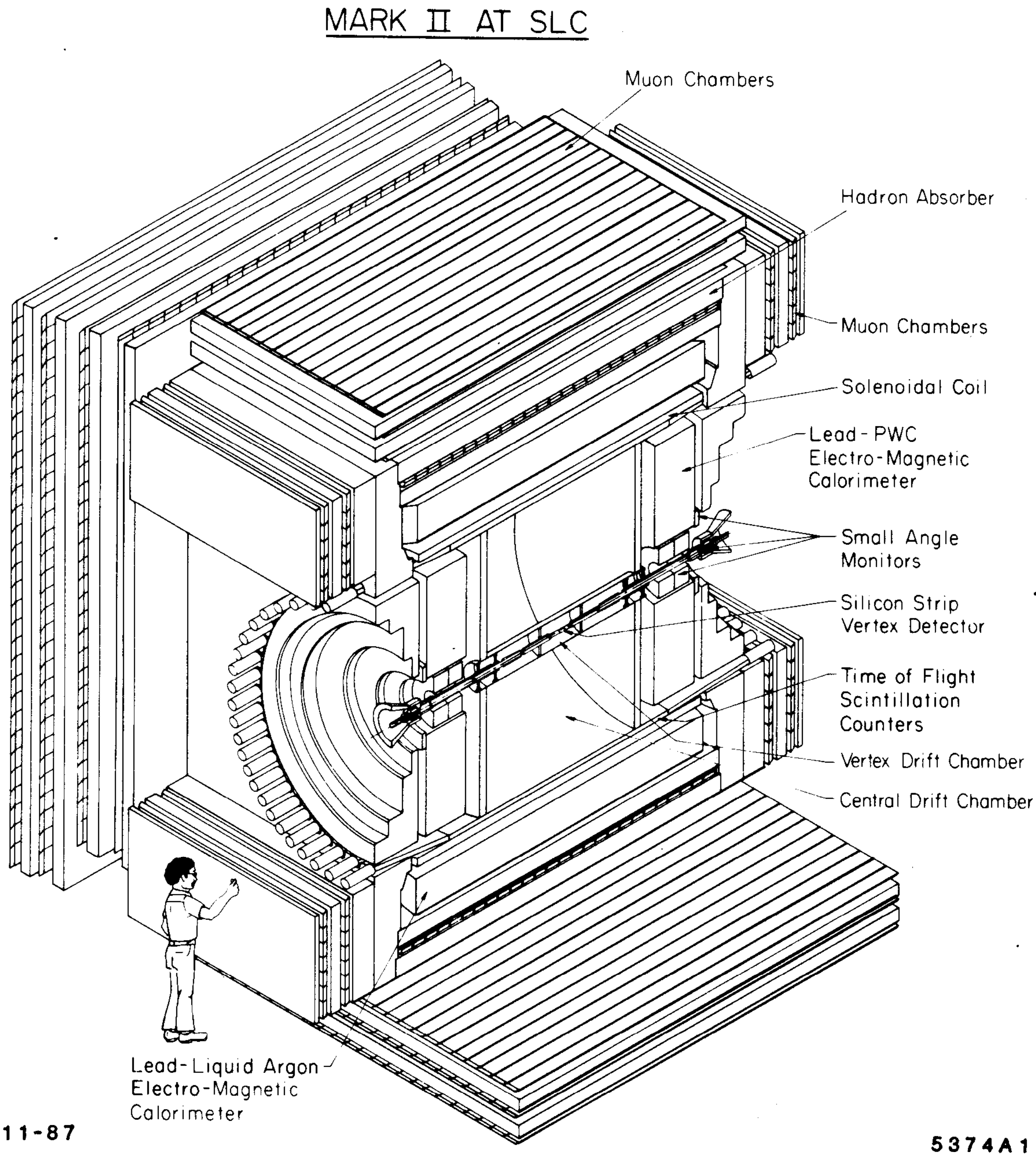

Fig. 11. An isometric view of the MARKII.

the forward direction. The small angle monitor (SAM) provides hermeticity in the 50–200 mrad region, the mini-SAM in the 15–25 mrad region and an instrumented mask in the region between these monitors. Additional cracks, like those

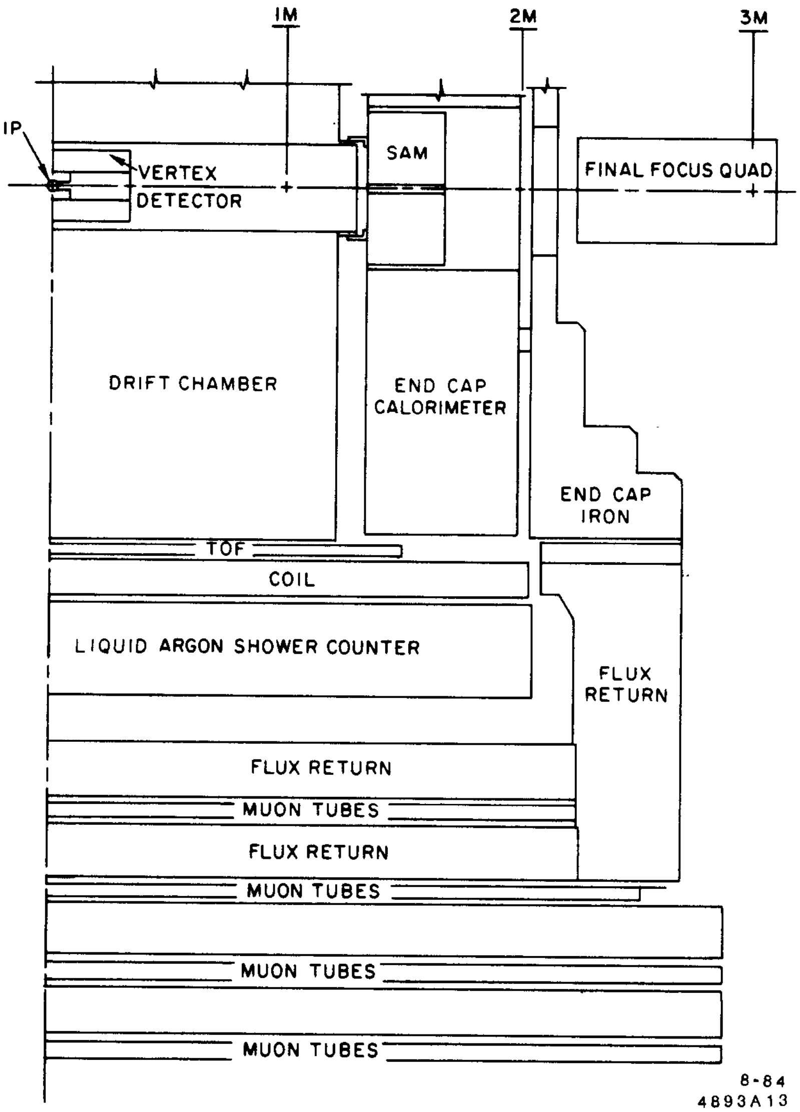

Fig. 12. A conventional view of one quadrant of the MARKII.

between the endcap and SAM (see Fig. 13) and between adjacent liquid argon barrel modules are covered by relatively crude shower counters, whose main design goal was efficient detection of electromagnetic energy, albeit with poor energy and spatial resolution. These devices therefore act as effective veto counters so that events with electromagnetic energy leaking through the cracks don't masquerade as missing energy events.

Muons are detected in a 4–layer system which covers 75% of the solid angle. Above 2 GeV/c, hadron rejection is at the 10^3 level in this system. The system is useful at momenta between 1 and 2 GeV/c only for isolated tracks. The time-of-flight system has a resolution of 250 picoseconds. Its role is to augment the dE/dx in the "overlap" regions, help with the isolation of cosmic ray events and provide discovery potential for slow (heavy) particles like possibly free quarks.

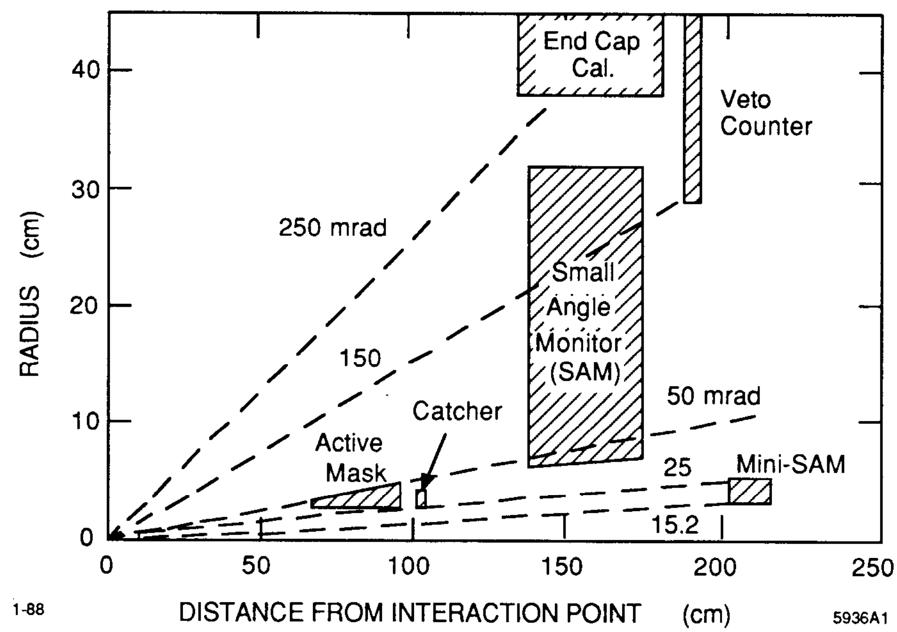

Fig. 13. Placement of the MARKII small angle detectors.

There are two vertex detectors, a high pressure drift chamber with 30 μm resolution (per wire) and 38 layers of wires plus a three layer silicon strip device with 5 μm resolution per layer. The inner-most silicon layer will be at a radius 2.5 cm. These devices are not yet installed in the MARKII—installation is expected in mid-1989.

Luminosity monitoring is achieved in the usual way using small angle Bhabha scattering (t channel $e^+e^- \rightarrow e^+e^-$). The cross section for the scattering falls off very rapidly with the angle relative to the incoming beam, $d\sigma/d\theta \sim \theta^{-3}$, and to lowest order in QED

$$\sigma_{LO} = \frac{16\pi\alpha^2}{5}(\theta_{min}^{-2} + \theta_{max}^{-2}) \quad .$$

In order to achieve a useful counting rate one must therefore place luminosity monitors at small angles. This placement has a further advantage of avoiding contamination from weak production, namely $Z^\circ \rightarrow e^+e^-$.

The MARKII detector has two luminosity monitors. The SAM is a precise monitor which has nine layers of proportional wire tracking preceding the shower counters. The tracking chambers permit one to define a well understood solid angle and thereby control systematics. The SAM covers the angular range of $50 < \theta < 200$ mrads and has a counting rate equal to the Z° decay rate. Systematic effects are expected to limit the measurement at the <2% level. A second, less precise monitor, the mini-SAM, covers the solid angle $15 < \theta < 25$ mrads and has a counting rate of approximately seven times the Z° decay rate. It provides a cross-check of the SAM and a higher rate which will make it useful as an on-line monitor.

The limiting error for the Z° mass and width measurements comes from the knowledge of the collision energy, E_{cm}. Typical systematic errors coming from other sources are at the <10 MeV level. The SLC machine itself does not have provision for a collision energy measurement with anything approaching this precision—the best absolute accuracy is < 300 MeV. To overcome this, the MARKII group has constructed and commissioned a pair of energy measuring spectrometers, one in the electron dump line (after collision the beams are dumped) and another in the positron dump line. These spectrometers are capable of measuring both beam energies on a pulse-to-pulse basis providing a collision energy error of <35 MeV/c^2 absolute (for M_z) and <30 MeV relative (for Γ_z). The principle involved is illustrated in Fig. 14. The beam passes through a horizontal bend magnet which generates a horizontal sweep of synchrotron radiation. Next, the beam encounters a precisely calibrated spectrometer dipole magnet which provides a vertical kick. Finally, the beam encounters a second horizontal bend magnet generating a second horizontal sweep of synchrotron radiation. The synchrotron radiation is monitored on a phosphorescent screen viewed by a digitizing camera system. Knowledge of the distance between the synchrotron stripes, the distance from the magnetic center of the spectrometer magnet to the digitizing screens and the spectrometer magnet $\int B d\ell$ provides the beam energy. Figure 15 shows the phosphorescent screen digitizing system. The distance between the stripes is 27 cm and the accuracy of location of each strip is 80 μm. A wire array directly in front of the screens provides fiducial markers for monitoring the system. The spectrometer magnet was very carefully made and a precision of $< 10^{-4}$ in $\int B d\ell$ was achieved in the laboratory. The field is monitored in situ with two independent systems (a flip coil and an NMR).

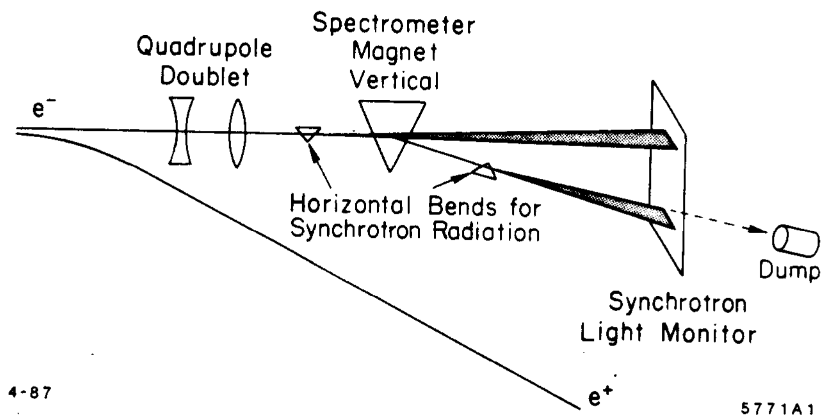

Fig. 14. Schematic drawing of the extraction line spectrometer for measuring the beam energy.

Table III summarizes the contributions to the absolute and relative errors arising from the spectrometers. All the entries are self-explanatory except possibly the last one. Motion of the beam coupled with the energy/position correlation of particles in the beam provide a systematic error correlated with the luminosity. Where the beams overlay fully, the total energy spectrum (as seen by the spectrometers) is contributing to the luminosity. However, if the beams move apart somewhat, lowering the luminosity, the energy spectrum of the collision is not the

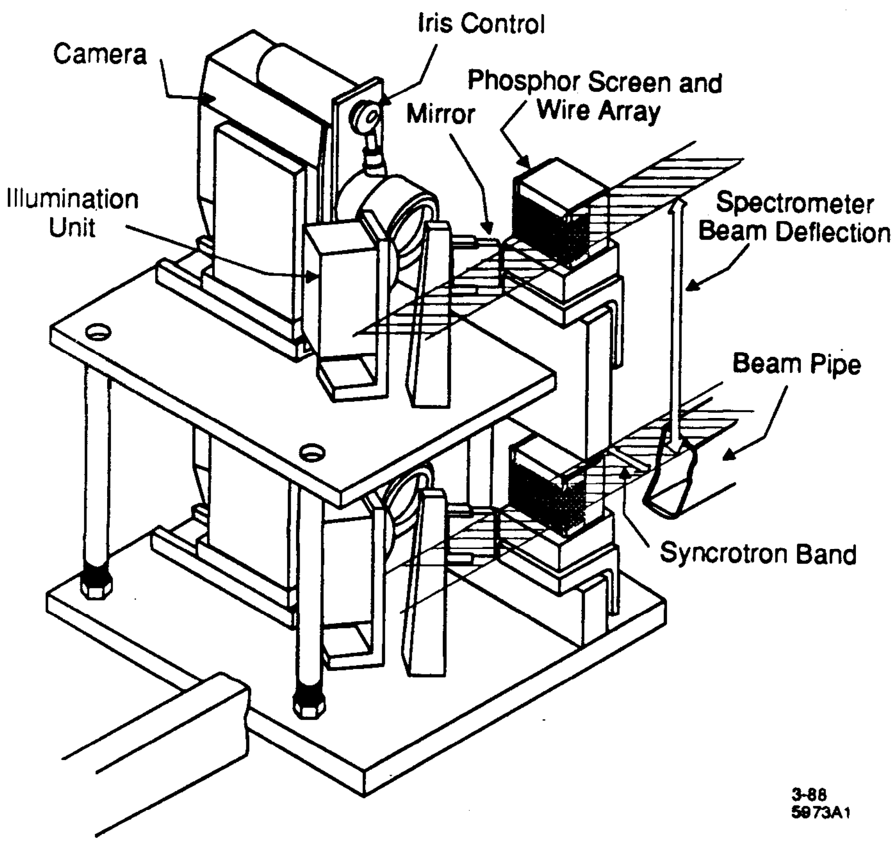

Fig. 15. Phosporescent screen synchroton light monitor system for the energy spectrometer.

same as measured by the spectrometer. This is the origin of the last contribution given in the table.

The spectrometers are fully operational devices and are read into the MARKII data acquisition system each event. On-line displays of the energy of each beam are available. A typical example of such a plot is given in Fig. 16. These spectrometers will play a central role in the initial SLC measurements.

Another SLC tool, not yet operational, is the availability of a polarized e^- beam. An electron beam with 45% polarization will be available at the collision point for running in 1990. The physics advantages of such a tool are discussed later.

Table III. Systematic errors in beam energy measurements.

Source of Error	Error in E_{cm} Relative MeV	Error in E_{cm} Absolute MeV
Laboratory field map	–	5
Monitoring field	5	5
X-ray detector localization of image (80 μ/27 cm)	15	15
Magnet alignment	–	5
Error in the single beam measurement	15 MeV	20 MeV
Error in the center-of-mass measurement	$\sqrt{2} \times 15$	$\sqrt{2} \times 20$
Beams at IP have an energy/position correlation	15	15
Total Error	30 MeV	35 MeV

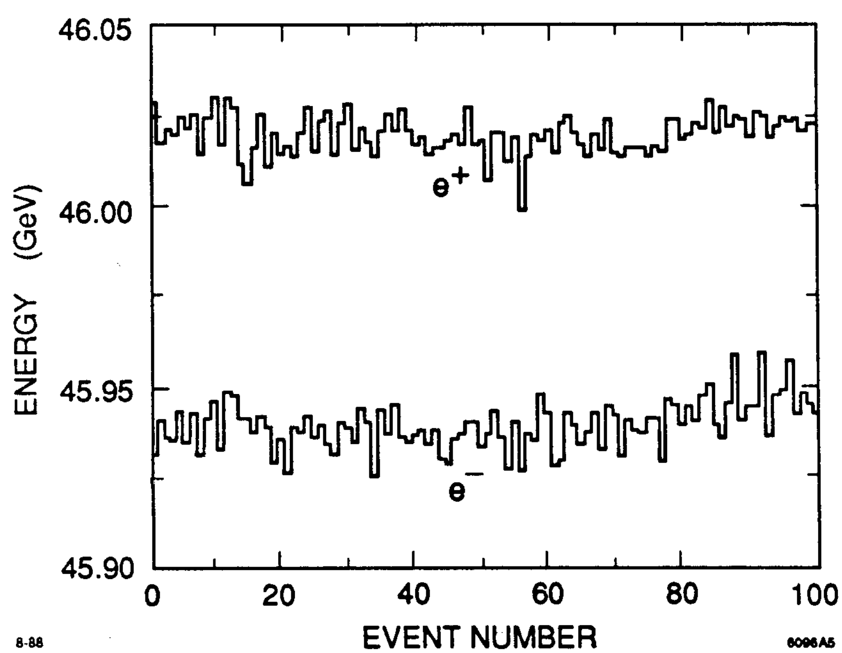

Fig. 16. Energy of the electron and positron beams as measured by the extraction line energy spectrometer over a period of a couple of minutes.

5. THE PHYSICS MEASUREMENTS

We have developed the theoretical background and discussed the measurables for testing the Standard Model. We have also given a brief description of the hardware available for the initial SLC running. It is now time to consider how the measurements will proceed and establish the precision with which information about Nature can be gleaned. As stated before, the simulations of the measurements have been done with the MARKII detector incorporating realistic analysis techniques and the generation of raw data which should therefore provide estimates of efficiencies and measurement errors which are close to what will be realized when data is available. Detailed discussions of these measurements can be found in Ref. 5(d).

5.1 The Z° Mass and Width

Clearly the first order of business is to measure the resonance line shape and extract the resonance parameters. This is relatively straightforward involving measuring the normalized Z° decay yield at a series of different collision energies, namely a scan in E_{cm} is performed. Presumably the scan energy will begin with our best knowledge of the Z° mass which at present is close to 92 GeV. This is based on the recent analysis of all the world's data, both from deep inelastic lepton scattering and the $\bar{p}p$ collider, which has been done by Amaldi et al.[6] They find a value of M_z (world average) = 91.8±0.9 GeV/c^2 which is very close to the UA2 measurement of 91.5± 1.2±1.7 GeV/c^2.

Because the Z° is rather wide (≈2.5 GeV), large scan steps (1–2 GeV) are appropriate. Figure 17 shows simulated experimental data for a scan. As discussed earlier, these data must be fit taking into account the effects of radiative corrections. Fortunately (see Ref. 4) Cahn[7] has come up with an analytic fitting function which extracts the resonance parameters, accounting for the radiative effects. Application of this fit introduces errors smaller than the measurement errors due to E_{cm}. Aside from statistics, the dominant error comes from the measurement of E_{cm}. With 100,000 Z° one achieves this systematic limit. The

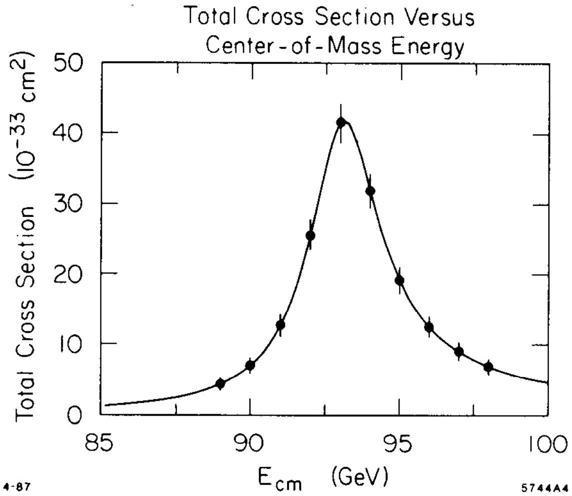

Fig. 17. A simulation of the data which would constitute a scan to map out the Z° line shape. The fit exhibits the clear asymmetry which arises from the initial state Bremsstrahlung.

Table IV. Expected precision for Γ_z and M_z as a function of the number of produced Z°'s. Statistical and systematic errors are added in quadrature. The error in $\sin^2\theta_w$ coming from δM_z is shown assuming Δr=0.07.

$\#Z^\circ$ Produced	Width $\delta\Gamma_z$(MeV)	Mass δM_z(MeV/c^2)	$\delta\sin^2\theta_w$ ($\Delta r = 0.07$)
5–10 K	60	65	0.0004
10–20 K	45	50	0.0003
100 K	30	35	0.0002

precision achieved for smaller data-sets is summarized in Table IV. One sees that even a modest sized data-set of 10,000 Z°'s provides an impressive measurement of both M_z and Γ_z; Γ_z will be known to almost a third of a neutrino generation.

With this level of precision for M_z, what do we learn about $\sin^2\theta_w$? Taking into account electroweak radiative corrections, as typified by the loop diagrams in Fig. 18, one finds

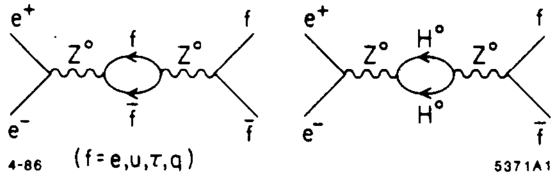

Fig. 18. One-loop weak radiative corrections to the process $e^+e^- \to Z^\circ \to f\bar{f}$.

$$\sin^2\theta_w = \frac{1}{2}\left\{1 - \left[1 - \frac{1}{(1-\Delta r)}\left(\frac{74.56}{M_z(\text{GeV})}\right)^2\right]^{1/2}\right\}$$

where $\Delta r = \Delta r$ (M_t, M_{H°, ... loop masses) is the contribution from the radiative corrections. The largest uncertainty arises from the t quark as discussed in Ref. 8 and summarized in Table V. Hence, lack of knowledge of Δr impedes extracting $\sin^2\theta_w$ from a measurement of M_z. However, if the t quark mass is known, the next largest effect is due to the Higgs mass, but this contributes a much smaller uncertainty to Δr. As an indication of the effective precision is $\sin^2\theta_w$ resulting from the M_z measurement, $\delta\sin^2\theta_w$ is given in Table V assuming $\Delta r = 0.07$ ($M_t =$ 50 GeV/c^2). So, an additional measurement of $\sin^2\theta_w$ will have to be made at the Z° in order to untangle the effects of radiative corrections.

Table V. Effect of the top quark mass on the size of the electroweak radiative corrections and thereby on $sin^2\theta_w$ (Taken from Ref. 8).

M_t GeV	Δr	$\sin^2\theta_w$
45	0.0713	0.230
90	0.0606	0.226
150	0.0412	0.219
200	0.0180	0.213

It is interesting to surmise what we can learn about M_t from an accurate measurement of M_z. Figure 19 is taken from Ref. 8 and plots contours of M_t versus M_z assuming the results from low energy data combined with a measurement of M_z good to $\pm$ 100 MeV/c^2. If one uses the UA1 top quark mass limit, and if $M_z > 93.5$ GeV/c^2, this scenario implies there must be physics beyond the Standard Model. If $M_z < 90.5$ GeV/c^2, M_t would have to be > 100 GeV/c^2.

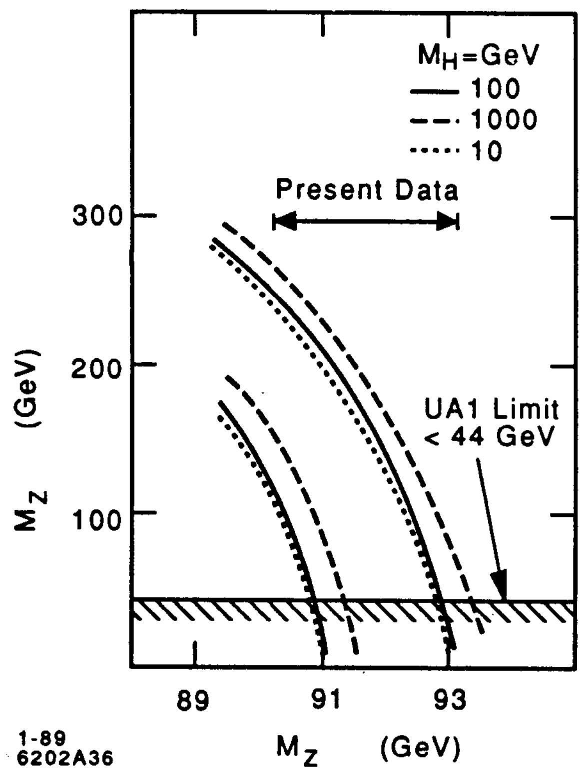

Fig. 19. Shown is a 90% C.L. range allowed for M_t by combining existing data with a measurement $M_Z = M_Z^{\text{expt}} \pm$ 100 MeV/c^2, shown as a function of M_Z^{expt} for three values of the Higgs-boson mass. Also shown are the UA1 limit $M_t > 44$ GeV and the 90% C.L. range $M_Z = 91.8 \pm 1.5$ GeV allowed by existing data. (Taken from Ref. 8.)

5.2 Measuring $\sin^2\theta_w$

We have seen that M_z does not provide a direct measurement of $\sin^2\theta_w$ because of the uncertainty in the size of the radiative corrections. Additional measurements of $\sin^2\theta_w$ are needed. Any measurement of a vector coupling measures

$\sin^2\theta_w$:

$$v_f = T_3^f - 2Q_f \sin^2\theta_w \quad .$$

We recall the forward-backward asymmetry provides such a measurement.

Consider first using the reaction $Z^\circ \to \mu^+\mu^-$. This has the advantage of a very simple, background-free topology. There is no need to identify the muons in the muon system because the only competing topological background is from $Z^\circ \to e^+e^-$. But this has a very distinctive signal in the electromagnetic calorimeter (a 50 GeV electron deposits about 42 GeV in the MARKII calorimeters while a 50 GeV muon deposits only 300 MeV/c) and hence the solid angle available for this measurement is set by the calorimeters (95% in the case of MARKII). The disadvantages of this channel are the small branching fraction (3%) and the small asymmetry (2% for $\sin^2\theta_w = 0.23$, 4% for $\sin^2\theta_w = 0.22$). In addition, the effects of the uncertainty in the collision energy are a large source of systematic error (see Fig. 7). Propagating the statistical errors one finds the precision in $\sin^2\theta_w$ as a function of the number of produced Z°'s in Table VI, where $\sin^2\theta_w = 0.22$ has been assumed. Large statistics are needed for a precision measurement of $\sin^2\theta_w$ from A^μ_{F-B} (or A^e_{F-B}).

Table VI. The statistical error obtained for $\sin^2\theta_w$ from measurements of the $\mu^+\mu^-$ and $b\bar{b}$ charge asymmetries.

# Z°'s Produced	$\delta\sin^2\theta_w$ from A^μ_{F-B}	$\delta\sin^2\theta_w$ from A^b_{F-B}
10^5	0.006	0.008
10^6	0.002	0.003

How about using quark pair asymmetries? The reaction $Z^\circ \to b\bar{b}$ is the most practical. The asymmetry is fairly large—11%—and the branching fraction for $Z^\circ \to b\bar{b}$ is also respectable at 13.6%. In contrast to the $\mu^+\mu^-$ channel, it is about a factor of 2–3 times more difficult to get a cleanly tagged $b\bar{b}$ sample. Also, as discussed in Chap. 3, this channel is only half as sensitive to $\sin^2\theta_w$ as $\mu^+\mu^-$, but the systematic error from δE_{cm} (see Fig. 7) is not large ($< 1\%$).

So the question arises as to how one tags $Z^\circ \rightarrow b\bar{b}$. One utilizes the fact that B mesons, which are produced when the $b, \bar{b}$ quarks fragment are long lived ($\tau \approx 1$ picosecond). The long B meson lifetimes generate secondary vertices in the detector. The presence of these secondary vertices can be used as an event tag by observing that the decay products at the secondary vertex do not extrapolate back to the primary vertex (see Fig. 20), but have a finite impact parameter: b. Simulations of the MARKII vertex detector system indicate that the efficiency for tagging a $b\bar{b}$ event using the large impact parameter secondaries is 40%. The fraction of (charm) background in this sample is less than 10% of the signal. The algorithm used requires the event to have ≥ 3 charged tracks with a measured impact parameter larger than $3\sigma_b$ (where σ_b is the impact parameter measurement error) and an invariant mass larger than 1.9 GeV/c^2 (to eliminate charm decays from $c\bar{c}$ events).

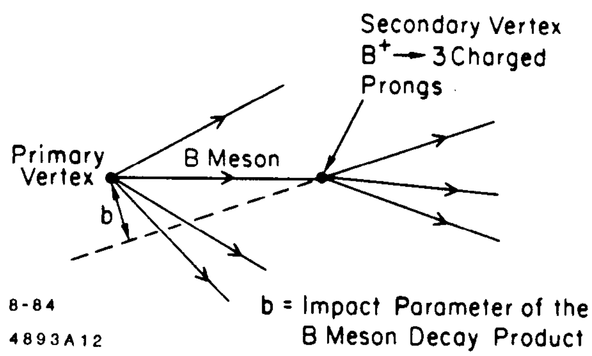

Fig. 20. The production and subsequent decay of a B meson indicating the primary vertex, secondary vertex and the impact parameter b of one of the B decay tracks.

In order to measure A^b_{F-B}, one must be able to distinguish the b from the $\bar{b}$. This is done by requiring a lepton in the event, the sign of the electric charge of the lepton tags that hemisphere as b or $\bar{b}$. From simulations which incorporate all of these requirements, one obtains errors for $\sin^2\theta_w$ given in Table VI. Again, large statistical samples are needed to get the required precision.

The path to a high precision measurement of $\sin^2\theta_w$ with relatively low statistics is via the use of a polarized e^- beam where one gains a statistical advantage of a factor of ~50. The measurement of interest is the left-right polarization asymmetry which is the difference between the total Z° cross section for left-handed electrons colliding with unpolarized positrons and for right-handed electrons colliding with unpolarized positrons:

$$\begin{aligned} A_{L-R} &= \frac{\sigma_L - \sigma_R}{\sigma_L + \sigma_R} \\ &= \frac{2P_{e^-} a_e v_e}{(a_e^2 + v_e^2)} \end{aligned}$$

where P_{e^-} is the e^- polarization (45%). $A_{L-R} = 7\%$ for $\sin^2\theta_w = 0.23$, 12% $\sin^2\theta_w = 0.22$. A_{L-R} is independent of the couplings of the final state fermions and hence it has the maximum statistical power since one can use all the visible Z° decays for this measurement. The measurement is relatively simple, namely measuring a total cross section, and the limiting systematic error turns out to be the error in the polarization. Two polarimeters are being constructed, one uses Möller scattering another Compton scattering. A 5% error in the knowledge of P_{e^-} is considered easy, 1% is possible but will be hard to achieve. As shown in Fig. 21, errors arising from the uncertainty in E_{cm} are negligible, $\Delta A_{L-R}/\Delta E_{cm} \approx$ .15%/100 MeV. The precision with which one measures $\sin^2\theta_w$ from A_{L-R} is given in Fig. 22 (along with the expectation from A^{μ}_{F-B}) as a function of the number of produced Z°'s. For δP_{e^-} of 3%, an impressive systematic limit is reached at $\delta\sin^2\theta_w \approx 0.0007$ with a sample of 10^5 Z°'s.

5.3 Additional Methods for Indirectly Sensing New Physics

The Z° width is a crucial indicator of physics beyond the 3-generation Standard Model—an anomolous width with respect to the Standard Model prediction immediately signals new physics. So far we have discussed one way to measure Γ_z,

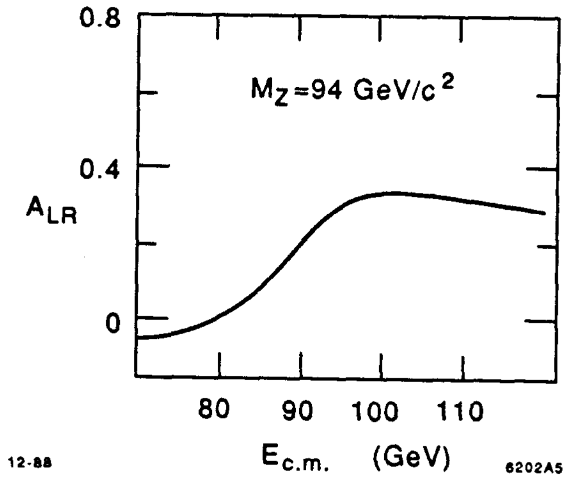

Fig. 21. The dependence of A_{L-R} on E_{cm}.

namely by mapping out the Z° line shape. It is interesting to ask whether we might have any cross checks of comparable accuracy as a way of verifying the direct measurement. It turns out that there are two measurements which can play this role; a)the so-called invisible width, Γ_{invis} and b) Γ_{tot} extracted from the cross section for $Z^\circ \to \ell^+\ell^-$ where $\ell^\pm$ are charged leptons.

Γ_{invis} is defined as the difference between the total width and the visible width:

$$\Gamma_{invis} = \Gamma_{tot} - \Gamma_{vis} \quad .$$

(Note that if Γ_{invis} is entirely due to neutrinos $N_\nu = 12\sqrt{2}\pi/G_F M_Z^3 \Gamma_{invis}$, where N_ν is the number of massless neutrino species in the world.) Γ_{vis} will get contributions from the charged leptons and the hadronic events, namely

$$\Gamma_{vis} = \Gamma_{e^+e^-} + \Gamma_{\mu^+\mu^-} + \Gamma_{\tau^+\tau^-} + \Gamma_{had} \quad ,$$

where Γ_{had} may well contain "new physics." We will assume (quite legitimately) that we can use the Standard Model to calculate $\Gamma_{\ell^+\ell^-} = G_F M_Z^3/24\sqrt{2}\pi(v_e^2 + a_e^2)$, leaving Γ_{had} to be measured. If we run on the Z° peak, Γ_{had} can be obtained by

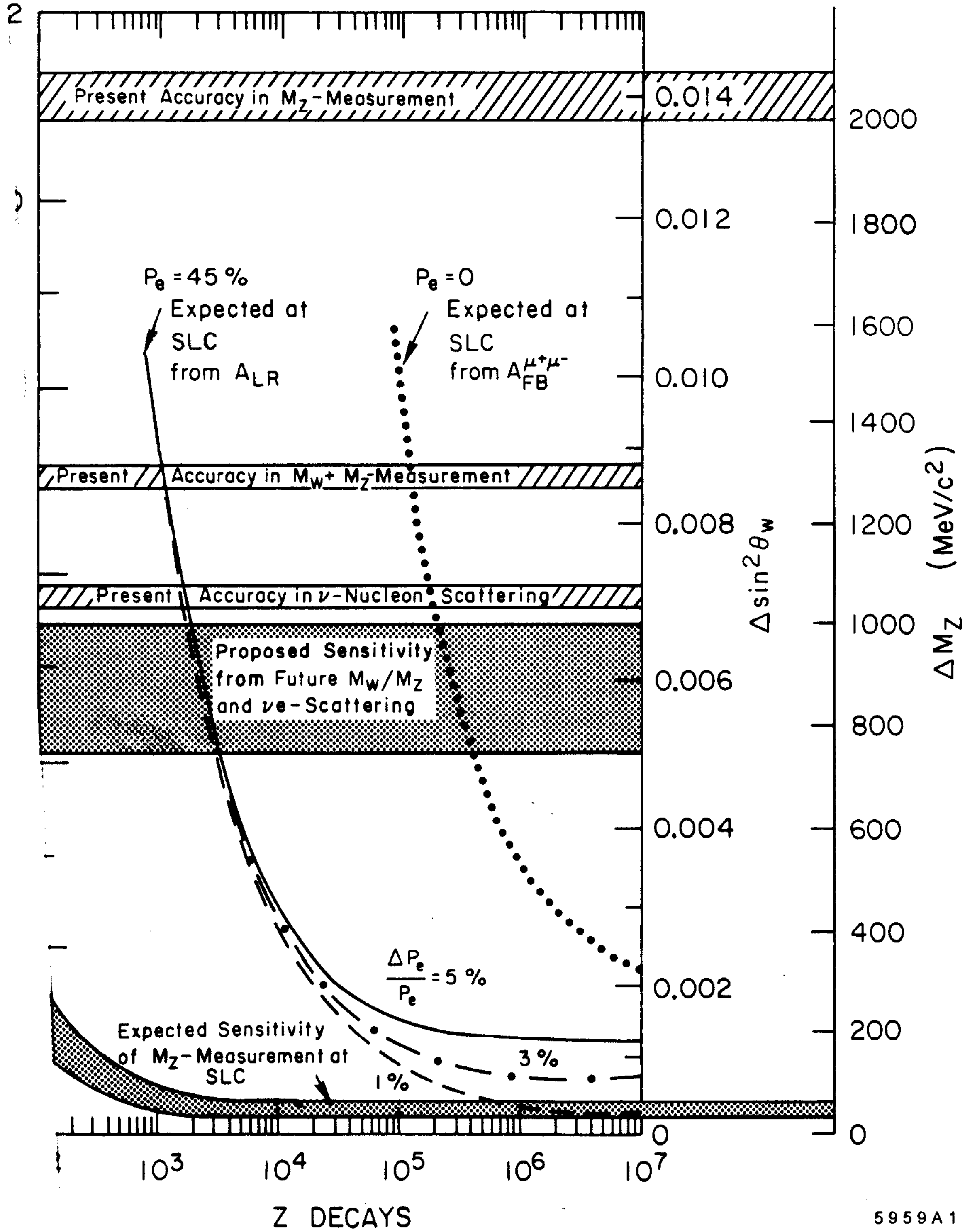

Fig. 22. The uncertainties in the determination of $M_Z, \sin^2\theta_w$, or A_{L-R} for various measurements which can be made at the SLC as a function of the number of observed Z° decays.

measuring the yield of hadronic events (N_{had}) and mu-pairs ($N_{\mu\mu}$):

$$\Gamma_{had} = \frac{N_{had}\epsilon_{\mu\mu}}{N_{\mu\mu}\epsilon_{had}}\Gamma_{\mu\mu} \quad .$$

In addition, recall from our theoretical discussion that

$$\Gamma_{tot} = \frac{\sqrt{12\pi}\Gamma_{\mu\mu}}{M_Z}\sigma_{\mu\mu}^{-1/2} \quad ,$$

where we can measure $\sigma_{\mu\mu}$ in a run with luminosity $\mathcal{L}$ as

$$\sigma_{\mu\mu} = \frac{N_{\mu\mu}}{\mathcal{L}\epsilon_{\mu\mu}} \quad .$$

Hence, if one measures the five quantities $N_{\mu\mu}, N_{had}, \epsilon_{\mu\mu}, \epsilon_{had}$ and $\mathcal{L}$, one can extract both Γ_{tot} and Γ_{invis}.

With some manipulation and patience the errors in Γ_{tot} and Γ_{invis} can be obtained:

$$\Delta\Gamma_{tot} = 0.5 \ \ \Gamma_{tot}\left\{\left(\frac{\Delta N_{\mu\mu}}{N_{\mu\mu}} \oplus \frac{\Delta\epsilon_{\mu\mu}}{\epsilon_{\mu\mu}}\right) \oplus \frac{\Delta\mathcal{L}}{\mathcal{L}}\right\}$$

$$\Delta\Gamma_{invis} = \left(-\frac{1}{2}\Gamma_{tot} + \Gamma_{had}\right)\left(\frac{\Delta N_{\mu\mu}}{N_{\mu\mu}}\right) \oplus \frac{\Delta\epsilon_{\mu\mu}}{\epsilon_{\mu\mu}} \oplus$$

$$\frac{1}{2}\Gamma_{tot}\frac{\Delta\mathcal{L}}{\mathcal{L}} \oplus \Gamma_{had}\left(\frac{\Delta N_{had}}{N_{had}} + \frac{\Delta\epsilon_{had}}{\epsilon_{had}}\right)$$

where the $\oplus$ symbol means add in quadrature. Because of the small branching fraction for $Z^\circ \rightarrow \mu^+\mu^-$, $\Delta N_{\mu\mu}/N_{\mu\mu}$ is the dominant error. Fortunately, it does not end up contributing significantly to $\Delta\Gamma_{invis}$ because of the small weighing factor $(-1/2\Gamma_{tot} + \Gamma_{had}) < 1/4\Gamma_{tot}$. Simulations have been performed to establish the precision with which the efficiencies will be known and yield $\Delta\epsilon_{Had} = 1\%$, $\Delta\epsilon_{\mu\mu} = 2\%$. We expect $\Delta\mathcal{L} = 2\%$; 3% has been used for the estimates which are summarized in Table VII as a function of the number of produced Z°'s. For these estimates it is assumed that all three lepton states, $\mu^+\mu^-, e^+e^-$ and $\tau^+\tau^-$ can be

Table VII. The measurement errors for Γ_{invis} and Γ_{tot} as a function of the number of produced Z°'s.

# Z°'s Produced	$\Delta\Gamma_{invis}$ MeV	$\Delta\Gamma_{tot}$ MeV
1,000	105	156
5,000	62	82
10,000	54	67

used for the measurement. One sees that for a 10,000 Z° sample size one has two powerful adjuncts to the 60 MeV width measurement obtained from fitting the line shape.

If there is an indication of an anomolous, width, we will know that there must be new physics. But of course we don't know specifically what the new physics channel(s) is. One has to look directly for the visible topologies in the detector. In addition it should be evident that heavy particles which are produced in pairs in the usual way, whose masses are close to (but smaller than) $M_z/2$, will make relatively small contributions to Γ_z. These contributions can easily be less than the experimental resolution. As examples, a 45 GeV/c^2 fourth generation b quark would only contribute 37 MeV to Γ_{tot}, a 45 GeV/c^2 t quark, 13 MeV. To discover such physics likewise requires topological searches. If the measured width is anomolous, and no evidence is found for non-standard events, one will then know that the additional width must arise from weakly coupled, stable neutral objects (i.e., neutrinos or sneutrinos) and confirmation would come from the Γ_{invis} measurement.

6. SEARCHING FOR THE TOP QUARK

There is not much phase space left for $Z^0 \rightarrow t\bar{t}$ searches since we have an unambiguous limit from TRISTAN of $M_t > 27.5\ GeV/c^2$ and a somewhat less direct limit from UA1 of $M_t > 41\ GeV/c^2$. If indeed there are only three generations, the Standard Model is pushing us in the direction of higher top quark masses; certainly $M_t < M_z/2$ is hard to accommodate in the three-generation

Standard Model. Nonetheless, unambiguous experimental measurements are the final arbiter and hence we will certainly search for the top quark. Indeed, if nature is kind and $M_t < M_z/2$, a relatively small data set of several thousand Z°'s will provide a clean signal.

There are several topological search procedures which have been studied. These procedures rely on the fact that the t quark is necessarily much heavier than the five known quarks. Clearly the background for the $Z^\circ \to t\bar{t}$ searches comes from the hadronic decays of the Z° into the five light quarks and more specifically from events which contain gluon radiation. These events can simulate the "fatter" $Z^\circ \to t\bar{t}$ kinematics. Two search methods are presented here: the use of event-shape parameters as an example of a poor technique and isolated leptons as an example of the search method of choice.

The reason that event-shape parameters are "dangerous" is that they are subject to our lack of understanding of the fragmentation process. Different Monte Carlo models, all tuned to adequately fit the PEP/PETRA data, do not provide reliable or consistent background predictions in the kinematic region (multi-jet events) of interest to these searches. The variable most useful for isolating $Z^\circ \to t\bar{t}$ is the aplanarity as defined in the sphericity tensor scheme. Aplanarity is a measure of the amount of momentum "out" of the event plane. Two-jet events from light quarks have very small aplanarity; light quark events can have large aplanarities due to gluon radiation. For the $Z^\circ \to t\bar{t}$ one naturally expects large aplanarities because of the heavy t-quark mass.

Table VIII summarizes the results of an analysis based on the use of aplanarity. For this simulation 10^4 events of the type $Z^\circ \to hadrons$ via the five known quarks were produced using three different QCD/fragmentation models and the events were reconstructed in the detector. A sphericity analysis was performed and events were excluded if the aplanarity was less than 0.12. The number of (background) events passing this cut are given in the first column of Table VIII. The problem alluded to above is now rather clear, namely the background estimates of the different Monte Carlo models vary by a large amount, especially when compared with the expected signal yields also given in Table VIII for different t quark mass assumptions. The number of $Z^\circ \rightarrow t\bar{t}$ events is normalized to the 10^4 Z° hadronic events using the branching fractions in Table II (with M_z assumed to be 93 GeV) augmented by the QCD radiative correction outlined in Ref. 9 and shown graphically in Fig. 23. One might argue that with enough hadronic Z decays, the Monte Carlos could be optimized to give a proper description of the Z° hadronic environment for the five known quarks. However, this cannot be done until one has a complete understanding of all the possible sources of hadrons, i.e., searches for new hadron sources must necessarily precede this optimization.

Table VIII. The search for top using the shape parameter aplanarity. The first column summarizes the contributions from the background for three different Monte Carlo models. Note the large variation in the predictions of the different models. The rest of the columns are the signal assuming different top masses.

M_t	# of Events Produced	# of Events with Aplanarity > 0.12
Background:		
Lund $0(\alpha_s^2)$	10^4 udscb	10 ± 3.5
Lund Leading Log	$(1.4 \times 10^4 Z^\circ)$	37 ± 5.6
Webber Shower		76 ± 9.0
40 GeV/c^2	512	112
42.5 GeV/c^2	372	82
45 GeV/c^2	240	40

In summary then, the method of shape parameters is a poor way to proceed. This statement is not just true for the aplanarity—all the potentially useful shape parameters suffer the same fate.

The use of large transverse momentum leptons, from quark leptonic decays, does not suffer from the uncertainties of fragmentation and is a clean, high

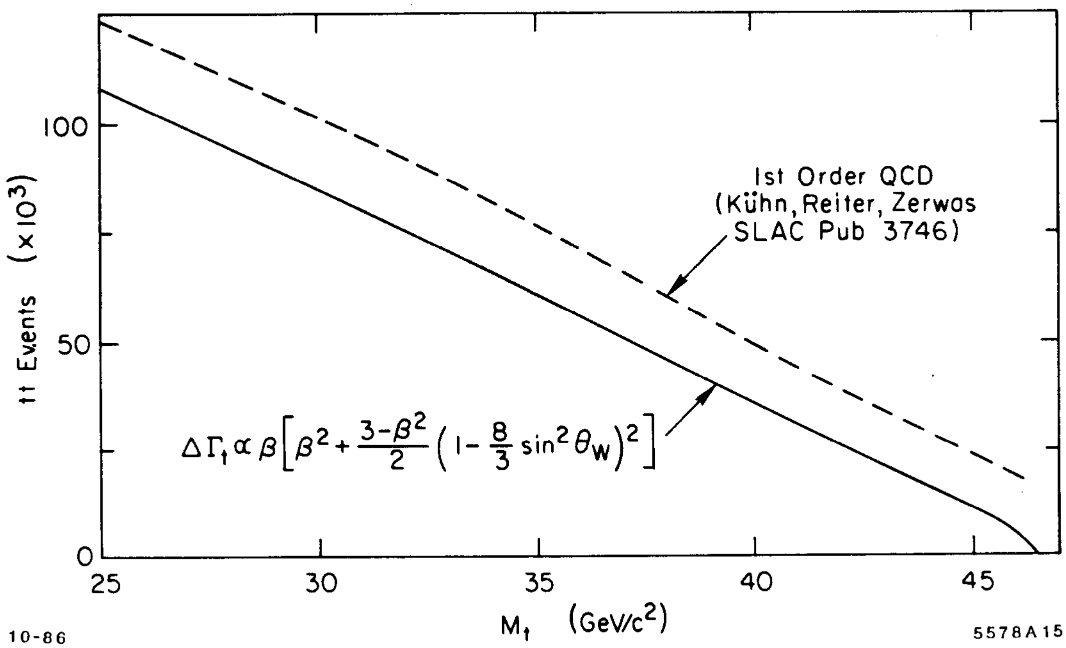

Fig. 23. The effects of QCD radiative corrections to the yield of $Z^\circ \to t\bar{t}$ events following the calculations of Ref. 9.

efficiency method of finding top at the Z°. The signal topology involves tagging isolated electrons and/or muons coming from the decay sequence $Z^\circ \to t\bar{t}$; $t \to b + e(\text{or } \mu) + \nu, \bar{t} \to$ hadron jets. Because of the large t quark mass, the resulting high momentum e and μ are often well isolated from the hadronic jets.

The background comes potentially from $Z^\circ \to b\bar{b}$; $b \to c + e(\text{or } \mu) + \nu, \bar{b} \to$ hadron jets. However, in this case, even when the e or μ have high momentum, they are not isolated from the hadronic jets.

A clean separation of the signal is obtained with relatively simple cuts which have good efficiency. Multiparticle events are selected which have a lepton (electron or muon) with transverse momentum (P_t) relative to the thrust axis larger than 3 GeV/c. The hadrons are then partitioned into jets using a cluster algorithm. The lepton isolation parameter is then calculated for each jet (j) as follows:

$$\rho_j = \{E_\ell(1 - \cos\theta_{\ell j})\}^{\frac{1}{2}} \quad ,$$

where E_ℓ is the lepton momentum and $\theta_{\ell j}$ is the angle between the lepton and the axis of the jth jet: ρ_j is effectively the invariant mass of the lepton-jet system assuming the jet mass to be 1 GeV/c^2. The lepton isolation parameter for the event is chosen as

$$\rho = min\{\rho_j\} \quad .$$

Figure 24 shows dn/dρ for a background sample of $10^4 Z^{\circ}$'s decaying to the five light quarks and for a sample of appropriately normalized $Z \rightarrow t\bar{t}$ events with $M_t = 40$ GeV/c^2. Both electrons and muons are used in this analysis and both the signal and background are subject to the selection criteria given above. A cut at $\rho > 1.8$ GeV$^{1/2}$ provides an efficient and clean $Z^{\circ} \rightarrow t\bar{t}$ signal. Predictions of the background spectrum have been verified to be independent of the QCD/fragmentation model as indicated in Table IX which summarizes the sensitivity of the selection technique for different t-quark masses. Again, $M_z = 93$ GeV/c^2 was assumed for these simulations.

The isolated lepton search procedure for $Z^{\circ} \rightarrow t\bar{t}$ is robust and particularly free of background. The efficiency is high enough that with 1,000 Z° events one would have a significant excess of events for $M_t \leq 43$ GeV/c^2, with 5,000 events one could explore the region very close to the kinematic threshold of $M_z/2$.

Having found the signal described above, how does one know that the source is $t\bar{t}$ as opposed to say $b'\bar{b}'$? The rate is not a useful means of separating these two possibilities, unless the mass is well known, QCD corrections are understood, and one has large statistics. It turns out that it is possible to distinguish these two scenarios as discussed in the next section.

There are several possible ways to measure M_t once one has a signal. These include counting the yield of high P_t leptons, fitting the shape of the P_t distribution, reconstructing the hadronic jet mass in the isolated lepton events... . All these methods suffer from one deficiency or another and yield typical mass uncertainties of about 2 GeV/c^2 for the mass range and event sample sizes ($\sim 10^4 Z^{\circ}$'s) discussed here. Presumably if a precise measurement of M_t was needed, one could lower the beam energy and scan for toponium using the crude mass measurement as an

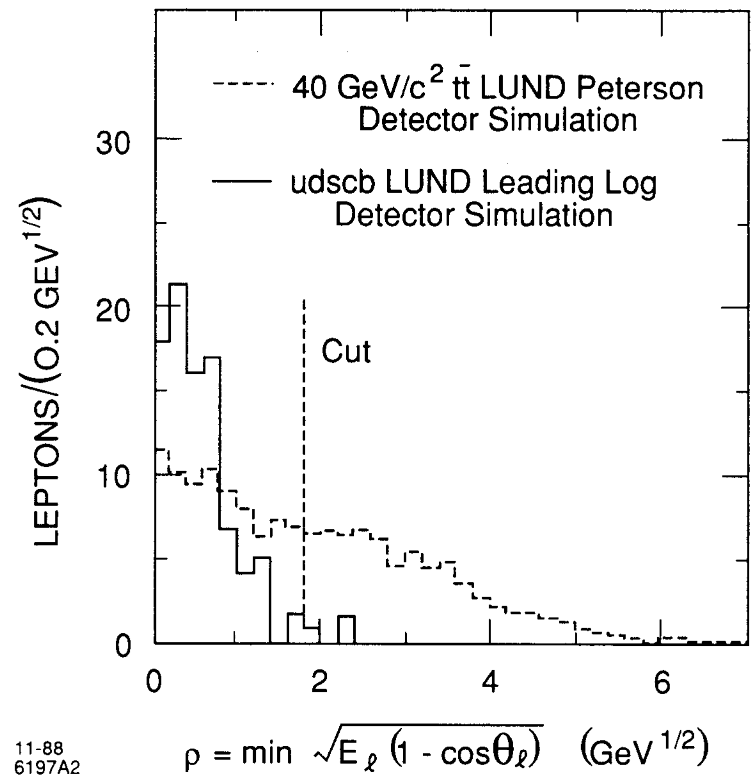

Fig. 24. Isolation criterion for leptons with $P_t > 3$ GeV/c. Distribution of ρ (defined in text) for leptons with $P_t > 3$ GeV/c for 10,000 udscb events from the Lund leading log model with full detector simulation and for 512 $t\bar{t}$ events with $M_t = 40$ GeV/c^2 from the Lund model with Peterson fragmentation.

indicator of where to scan. A relatively large luminosity ($\approx 10^{30}\text{cm}^{-2}\text{sec}^{-1}$) will be needed to find toponium in a reasonable time. In addition, if the toponium mass is very close to $M_z/2$, interference effects greatly distort the toponium shape and make it impossible to find.[5d]

In conclusion, the Z° resonance is an excellent place to search for top as long as it is sufficiently low in mass to be produced. With 10,000 Z° events one would have sensitivity to masses up to $M_z/2$. The possible confusion between a top quark and a b' quark is easily resolved. Mass estimates in the range of $\pm$ 2 GeV/c^2 are possible.

Table IX. The search for top using the isolation criteria described in the text. The first column summarizes the contributions from the background for two different Monto Carlo models. The rest of the columns are the signal assuming different top masses. As described in the text, $\rho > 1.8$ GeV/c^2 and $P_t > 3$ GeV/c are the primary analysis cuts for the isolated lepton.

	# of Events Produced	# of Isolated Lepton Events	Signal: Background
Background: Lund Leading Log Webber	10,000 udscb ($1.4 \times 10^4 Z^{\circ}$'s)	2.6 ± 1.5 3.3 ± 1.9	
$M_t = 40$ GeV/c^2: Lund Symmetric Webber	512	76 ± 2.2 74 ± 4.3	25:1
$M_t = 42.5$ GeV/c^2 Lund Symmetric Lund Petersen	372	61 ± 4.7 62 ± 1.5	20:1
$M_t = 45$ GeV/c^2	240	38 ± 3.1	13:1
$M_t = 46$ GeV/c^2	195	30 ± 2.4	10:1

7. IS THERE A FOURTH GENERATION?

There are four obvious ways to search for a fourth generation of quarks and leptons:

1. Find a Q $= -1/3$ quark and demonstrate that indeed it is a Q $= -1/3$ quark (i.e., its not the top quark).
2. Find a 4th charged lepton.
3. Measure the number of massless neutrino species to be > 3.
4. Find a massive, neutral lepton.

It is entirely possible that a 4th generation exists and that all of its charged members are too heavy to produce at the Z°. In this case one would have to rely on the

ν counting experiments discussed in the previous section. This is also not infallible if the neutrino for the 4th generation is massive. Indeed the only way for a 4th generation to escape detection at the SLC would be if all its members had masses $> M_z/2$. We now consider the four possibilities suggested above.

7.1 Searching for a Fourth Generation $Q = -1/3, b'$ Quark

Clearly the isolated lepton technique discussed for the top quark search in the previous section works equally well for the b' quark. These studies have been done and the same level of efficiency and cleanliness is achieved for b' as for t. The issue then becomes whether these two possibilities are distinguishable?

In the absence of a good measurement of the quark mass and reliable QCD radiative corrections to the production cross section, using the absolute rate will not be useful. However, if we assume that $M_{b'} < M_t$ (which is a safe assumption for this scenario), b' decays are distinguishable from t decays because they result in a lot of leading charm (D*'s) which is not true for t decays:

$$b' \to c + W \qquad\qquad t \to b + W \quad .$$

The b from the t will decay to charm, but these charm jets will not produce leading D^*'s. So the trick for distinguishing b' jets from t jets is to tag $D^{*\pm}$'s which carry a large fraction of the beam energy. D*'s can be tagged using the famous ΔM technique, but this method has a very low efficiency since specific low branching fraction modes of the D^o enter. As discussed in Ref. 10, an inclusive D* tag is possible if one recalls that the bachelor pion in the decay $D^{*\pm} \to \pi^{\pm} D^o$ has very little momentum transverse to the D* flight direction ($< P_t^{\pi} > \sim 30$ MeV/c). This can be contrasted with the typical fragmentation pion which has $< P_t >$ of 300 MeV/c. We use this low P_t as an inclusive tag for charm.

In order to make this tag useful for separating t and b', one must remove contamination coming from $Z \to b\bar{b}, c\bar{c}$. This can be done by making a series of cuts which favor the heavy quark events and discriminate against slow D*'s; the full details can be found in Ref. 10. Multihadronic events are partitioned into jets using a cluster algorithm. Events with the event thrust > 0.9 are rejected. This cut favors the heavy quark events and discriminates strongly against $Z^\circ \rightarrow c\bar{c}$. Each charged track's P_t is measured relative to the axis of the jet to which it belongs. A further cut is made for candidate bachelor pions requiring them to have $Z = E^\pi/E_{cluster}$ between 0.04 and 0.08 where E^π and $E_{cluster}$ are the charged particle and cluster energy, respectively. This requirement discriminates against D* produced in b quark decays in which the bachelor pions are softer than these cuts permit. Figure 25(a) shows the P_t^2 spectrum for charged particles in a sample of 500 events of the type $Z \rightarrow b'\bar{b}'$ ($M_{b'} = 45$ GeV/c^2). The events and charged particle candidates satisfy the criteria discussed above. One sees the clear excess of low P_t tracks coming from the D*'s superimposed on the typical fragmentation spectrum with slope $\sim$ 300 MeV/c. Figure 25(b) shows the same distribution for a sample of $Z^\circ \rightarrow t\bar{t}$ events ($M_t = 45$ GeV/c^2) for which no hard D* component can be seen. Finally, Fig. 25(c) shows the P_t^2 distribution for a sample of 10^4 decays of Z° to the five light quarks plus 500 $Z^\circ \rightarrow b'\bar{b}'$ decays. One sees that, even in the presence of the "standard physics", the tagging technique has sufficient signal-to-noise to distinguish between a $Z \rightarrow b'\bar{b}'$ and $Z \rightarrow t\bar{t}$ scenario. Thus, these two scenarios are distinguishable. It is worth noting that this inclusive method is about 10 times more efficient than the more standard ΔM method.[10] In the same data set of 500 $b'\bar{b}'$ events, 125 tagged $D^{*\pm}$ are found [Fig. 25(a)]. Applying the ΔM method and using as many D^o decay modes as possible one finds 12 exclusively tagged events.

If $M_{b'} < M_z/2$, the b' quark is easily discovered at the SLC and it is distinguishable from the t quark.

7.2. Searching for a Conventional Fourth Generation Charged Lepton

We consider, for the moment, a conventional charged heavy lepton with a massless neutrino partner. The production rate is relatively small, $BF(Z^\circ \rightarrow L^+L^-) = 3\% f(\beta)$ where $f(\beta)$ is given in Sec. 3 and β is the $L^\pm$ velocity. $f(\beta) \rightarrow \beta^3$ as $M_L \rightarrow M_z/2$, which greatly limits the production for $L^\pm$ masses close to the

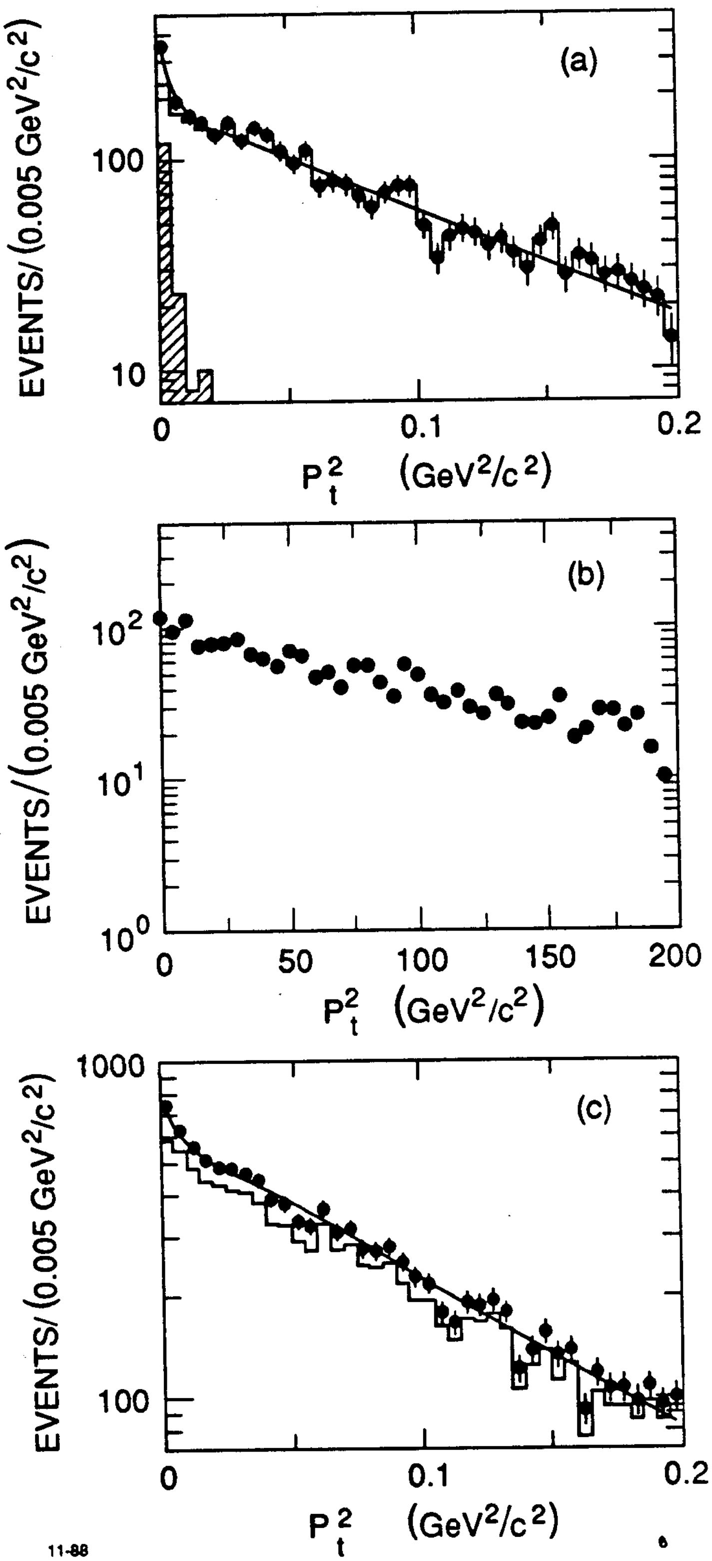

Fig. 25. (a). P_t^2 distribution for bachelor pion candidates (data points) obtained in the decay of a 45 GeV b' quark. The solid histogram corresponds to candidates not coming from a D^* and the hatched histogram to candidates coming from a D^*. The solid line is a fit to the data with two Gaussians, one of slope $\sim$ 30 MeV/c, the other $\sim$ 300 MeV/c. (b). The same as 25(a) except for a sample of $Z^\circ \rightarrow t\bar{t}$ with $M_t = 45$ GeV/c^2. (c). P_t^2 distribution for bachelor pion candidates (data points) obtained in 10,000 Z° decays containing 500 $b'\bar{b}'$ events. The histogram corresponds to only normal Z° decays (udscb). The solid line corresponds to the fit of two Gaussians to the total sample.

kinematic limit. We will assume that the $L^{\pm}$ decays via the standard weak interaction which means (ignoring QCD corrections which are small) that $BF(L^{\pm} \rightarrow \ell^{\pm}\nu\nu) = 11\%$ and $BF(L^{\pm} \rightarrow hadrons) = 67\%$.

Events containing a pair of acoplanar leptons ($e^{\pm}\mu^{\mp}$ for example) would constitute an unambiguous signal. For small data sets this is impractical because of the low statistical yield; only a handful of events are produced per 10^5 Z°'s. Hence, one must utilize the larger branching fraction modes involving hadrons.

Two topologies are envisaged as shown in Fig. 26. We refer to them as the 1+N and N+N topologies as described in the figure caption. Clearly these topologies (more particularly the N+N topology) will potentially have large background from the standard $Z^{\circ} \rightarrow$ hadrons events. In order to limit this background the analysis makes use of the substantial energy carried away by the neutrinos in the $Z^{\circ} \rightarrow L^{+}L^{-}$ events by requiring large missing energy. This is effective but the level of background is now model dependent. Applying an analysis of this type to the MARKII detector, one finds the signal to noise ratios given in Table X for two choices of $L^{\pm}$ mass. Both the N+N and 1+N topologies were used for this analysis and the data sample size was 20,000 produced Z°'s.

Table X. Signal and Background yields for the $Z^{\circ} \rightarrow L^{+}L^{-}$ search described in the text. These numbers correspond to 20,000 produced Z°'s.

	M_L = 30 GeV/c^2	M_L = 40 GeV/c^2
Signal	42	10
Background	1.5	< 1

Another analysis was done using only the 1+N topology, thus alleviating the concern about the model dependence of the background. Figure 27 gives the 90% confidence upper limit obtained for the $L^{\pm}$ mass as a function of the number of produced Z°'s.

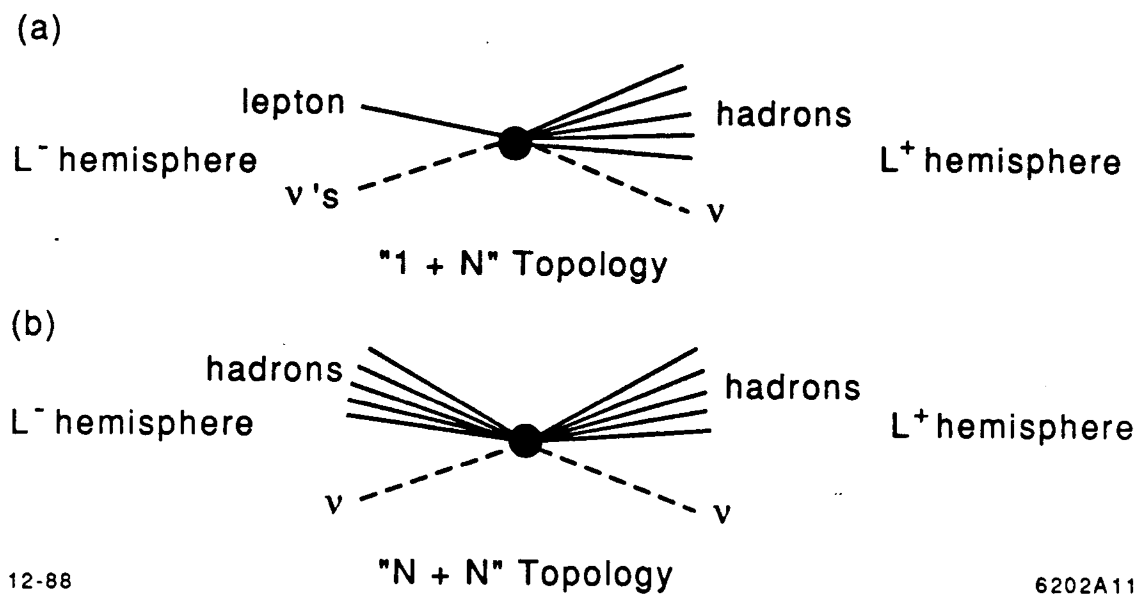

Fig. 26. Decay topologies used to search for $Z^{\circ} \rightarrow L^{+}L^{-}$.

If a 4th generation $L^{\pm}$ exists with a mass below $M_z/2$, it can be discovered at the SLC. A data set of $\sim$ 50,000 Z°'s is needed to cover the full mass range.

7.3. Searching for a Heavy Neutral Lepton

We consider now the example of a 4th generation doublet

$$\begin{pmatrix} L^{\pm} \\ L^{o} \end{pmatrix} ,$$

in which the L^{o} is massive. The production of the neutral partner is in pairs, namely $Z^{\circ} \rightarrow L^{o}\bar{L}^{o}$, for which the branching fraction is $BF(Z^{\circ} \rightarrow L^{o}\bar{L}^{o}) = 6\%$ $[0.25\beta(3+\beta^{2})]$, where β is the L^{o} velocity.

There are several scenarios to consider depending on the L^{o} and L^{-} relative masses.

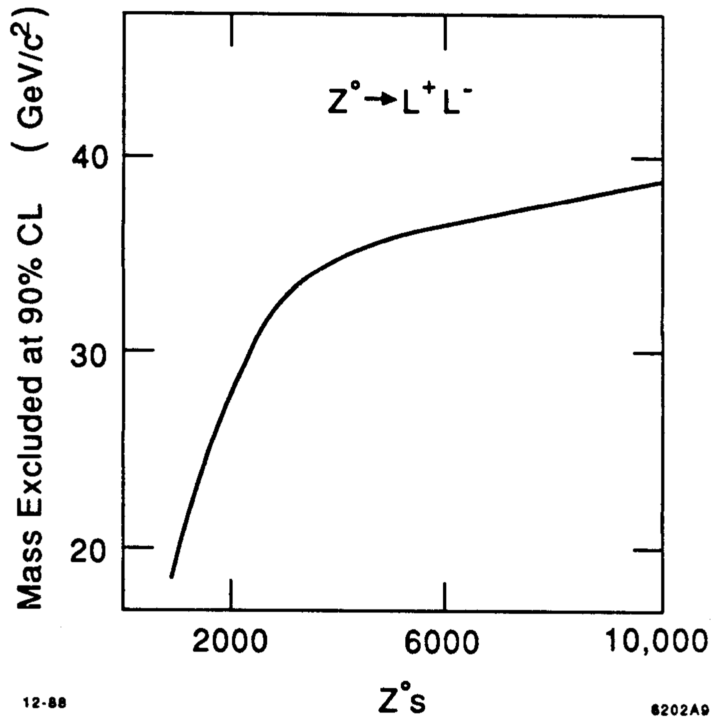

Fig. 27. 90% confidence limits on the $L^{\pm}$ mass as a function of the number of produced Z^{o}'s. The analyses strategy is explained in the text.

1. If $M_{L^o} < M_{L^\pm}$, the L^o is stable and will contribute to Γ_{invis} as discussed earlier. The amount it contributes depends on its mass, $\Delta\Gamma_{invis} = 1600.25\beta\,(3+\beta^2)]$ MeV.

2. If $M_{L^o} > M_{L^-}$ then $L^o \to L^- W^+$ is possible and L^- will be stable. If this were indeed the scenario the $Z^o \to L^o \bar{L}^o$ events would have a striking signature in which each hemisphere would contain the hadronic fragments of the W decay plus as penetrating heavy "muon-like" particle. This "heavy muon" would easily be distinguished from the familiar low mass muon in both the TOF and dE/dx detectors. Such a signal topology would be unmistakable. This scenario also produces events of the type $Z^o \to L^+L^-$ which for the same reasons of two back-to-back "heavy muons", has an unmistakable signature.

3. The L^o could also decay by mixing with a lighter generation(s) as indicated in Fig. 28(a). The mixing strength ($U_{\ell 4}$) determines the L^o lifetime:

$$\tau_{L^o} = \tau_\mu (\frac{M_\mu}{M_{L^o}})^5 \frac{BF(L^o \rightarrow L^+ \nu \ell^-)}{\mid U_{\ell 4} \mid^2} \quad ,$$

where ℓ^- stands for τ^-, μ^- or e^-. It would be most probable that the mixing would occur with the τ, but there is no reason to exclude e or μ. The measured properties of the τ (or e and μ) constrain the amount of mixing allowed which in turn puts lower limits on τ_{L^o}. It is not unreasonable to expect the L^o to have a decay length of at least several multimeters. Of course if the mixing is very weak (and/or the mass is relatively small) the decay length could exceed the size of a detector. This decay scenario leads to striking signatures with no conventional backgrounds. The distinctive features are low multiplicity multiple and mixed type leptons with displaced vertices [see Fig. 27(b) and (c)]. The two interesting topologies are (a) four-charged particle events in which the W's both decay leptonically which occurs about 10% of the time and (b) events with two charged particles in one hemisphere and a jet of hadrons in the other hemisphere which occurs about 40% of the time. The unusual mix of lepton types on the low-multiplicity side, coupled with the displaced vertices, will make these events unmistakenly anomolous. If indeed these heavy neutral leptons exist with masses below $M_z/2$, a few thousand produced Z^o's is all that one needs to discover them.

We can summarize the search for a 4th generation as follows:

1. b': is easily discovered in $< 10^4$ Z^o if it can be produced.

2. $L^\pm$: if stable easily discovered; if unstable clear search topologies exist and $\lesssim$ 50,000 Z^o's are needed to cover the full mass range.

3. L^o: if stable it will contribute to Γ_{invis}; if unstable it is easily discovered with $\sim$ few 1000 Z^o's.

4. $\nu_{L^\pm}$: a conventional, massless 4th generation neutrino will show up in the neutrino counting measurements of Γ_{tot} and Γ_{invis}.

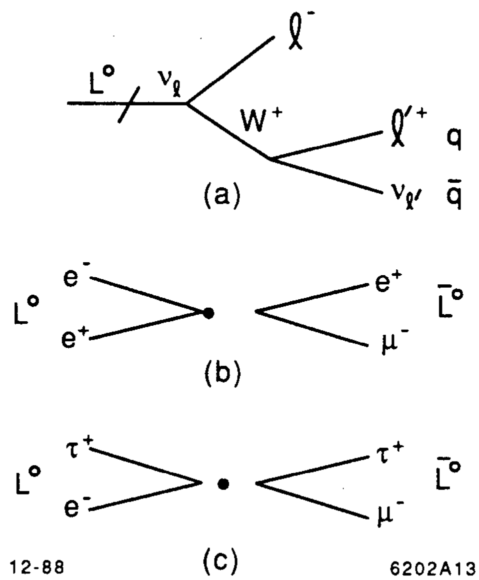

Fig. 28 (a) Schematic for L° decay by mixing with a lighter generation, (b) and (c) Event topologies used in the search for $L^\circ \bar{L}^\circ$.

The only way for the 4th generation to elude detection at the SLC is if *all four* of the members have masses $> M_z/2$.

8. SEARCHING FOR HIGGS SCALARS

At the Bonn Conference in 1981, Okun said that in his mind the outstanding experimental challenge was the search for scalars. He urged experimentalists to "drop everything" and devise cunning searches for the elusive scalars. To date no search has proven successful and it is interesting to speculate how one could search for the Higgs particles running at the Z^0.

The H^0 will couple to the heaviest fermions available and this feature will be used in any search for the H^0. The decay rate for $H^0 \to f\bar{f}$ is given by:

$$\frac{d\Gamma}{d\Omega} = \frac{G_F M_{H^0} m_f^2}{16\pi^2\sqrt{2}} \quad .$$

The decay rate depends on m_f^2 (m_f is the fermion mass) and is isotropic. So if $M_{H^0} < 2M_b$, the H^0 will decay mostly to $c\bar{c}$ and $\tau^+\tau^-$. If $2m_t < M_{H^0} < 2M_b$ then the H^0 will decay mostly to $b\bar{b}$. These conclusions are summarized in Fig. 29.

How can we search for the H^0? The process $e^+e^- \to Z^0 \to H^0H^0$ is forbidden by spin-statistics. The process $Z^0 \to H^0\gamma$ vanishes in first order because the Z° and γ are "orthogonal"—in second order the rate is too small to be of any practical use. The most promising search channel seems to be $Z^0 \to H^0 Z^{0*} \to H^0\ell^+\ell^-$ (see Fig. 30) which was first discussed[11] by Bjorken and is also discussed in Ref. 12. The rate for this process is given by:

$$\frac{1}{\Gamma(Z^0 \to \mu^+\mu^-)} \frac{d\Gamma(Z^0 \to H^0\ell^+\ell^-)}{dM_{\ell^+\ell^-}} = \frac{\alpha F}{4\pi \sin^2\theta_w \cos^2\theta_w}$$

where

$$F = \frac{10k^2 + 10\lambda^2 + 1 + (k^2 - \lambda^2)[(1 - k^2 - \lambda^2) - 4k^2\lambda^2]^{1/2}}{(1 - k^2)^2}$$

$$M_{\ell^+\ell^-} = \text{lepton pair mass}$$

$$k = M_L/M_{Z^0}$$

and $$\lambda = M_{H^0}/M_{Z^0} \quad .$$

This relative rate, integrated over $M_{\ell^+\ell^-}$, is plotted as a function of M_{H^0} in Fig. 31. Also shown for comparison is the rate for $Z^0 \to H^0\gamma$. $BF(Z^0 \to \mu^+\mu^-) = 3\%$, so one sees that for $M_{H^0} \approx 20$ GeV/c^2, $BF(Z^0 \to H^0\ell^+\ell^-) \approx 3 \times 10^{-5}$, a yield of 30 events for 10^6 Z^0 events. Unfortunately, the rate drops off very rapidly with increasing H^0 mass and for masses above ~ 40 GeV/c^2 the measurement becomes severely rate limited.

The $H^0\ell^+\ell^-$ signal must be sought in the presence of an enormous background from $Z^0 \to$ hadrons. For $M_{H^0} \approx 20$ GeV/c^2 there are $\approx 10^4$ $Z^0 \to$ hadron events per $Z^0 \to H^0\ell^+\ell^-$ event! Luckily the event topology is very favorable and a measurement indeed seems possible. Many of the detector groups[5] at SLC and LEP have studied the experimental problems and their conclusions are pretty uniform. We chose here in the MARK II study.

The favorable topology arises from the fact that most of the energy in the process $Z^0 \to H^0\ell^+\ell^-$ goes to the virtual Z^0 and hence the two leptons which result

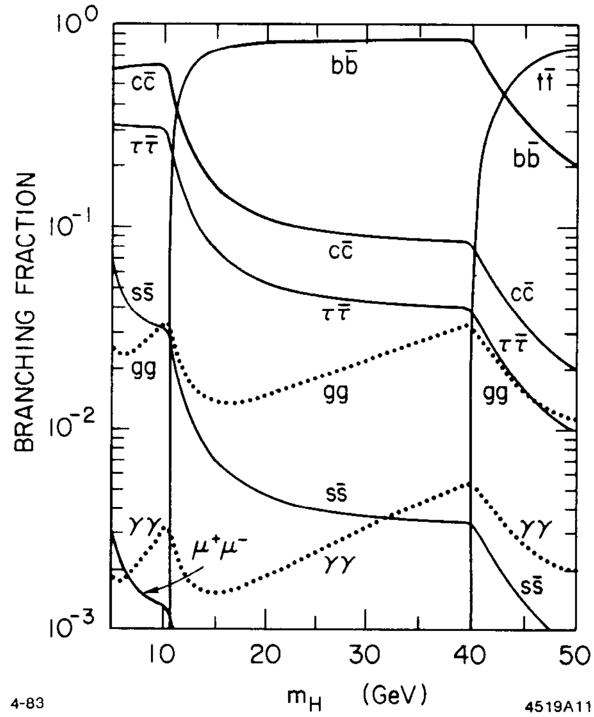

Fig. 29. Decay modes of the neutral Higgs boson as a function of its mass.

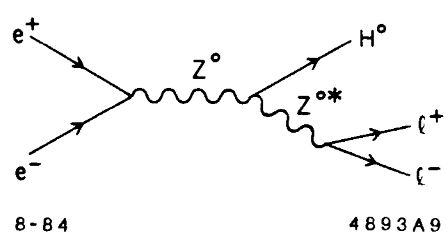

Fig. 30. The process $e^+e^- \rightarrow Z^0 \rightarrow H^0\ell^+\ell^-$.

from the decay of the virtual Z^0 have very high invariant mass and momenta. The H^0 is produced with a fairly small fraction of the available energy and will decay mostly into two quark jets. In addition there is very little correlation between the H^0 direction and the e^+ or e^- direction and in most events the $e^\pm$ will be well

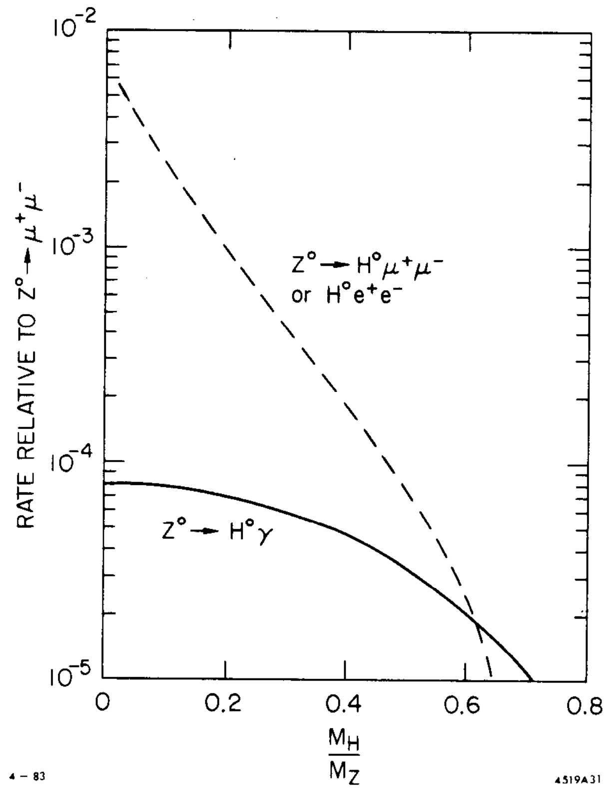

Fig. 31. The decay rate for $Z^0 \to H^0 e^+ e^-$ or $Z^0 \to H^0 \mu^+ \mu^-$ relative to $Z^0 \to \mu^+ \mu^-$ which has a branching fraction of 3%.

separated from the H^0 decay products. The topology is schematically shown in Fig. 32.

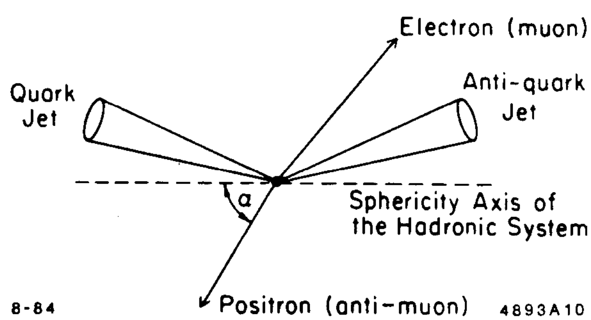

Fig. 32. A schematic representation of the topology of the $Z^0 \to H^0 \ell^+ \ell^-$ events.

The main source of background comes from the process $Z^0 \to t\bar{t}$ where both the t and $\bar{t}$ decay semi-leptonically. However, requiring the angle between the sphericity axis of the hadronic system (all particles except the ℓ^+ and ℓ^-) and the leptons to be $\gtrsim$ 200 mrad virtually eliminates this background for $M_{H^0} \lesssim$ 40 GeV/c^2. This cut loses very little signal ($\approx 6\%$) because there is virtually no correlation between the direction of the leptons and the hadronic sphericity axis. A small residual background from two photon production exists as discussed below.

The mass of the hadronic system (the H^0) is obtained from the missing mass recoiling against the lepton pair. The experiment can be done with either a e^+e^- or $\mu^+\mu^-$ lepton pair providing that the energy resolution of the leptons is sufficiently good to see a peak in the missing mass. The missing mass recoiling against the e^+e^- pair is shown in Fig. 33 for the MARK II simulation for Higgs masses of 10, 25, and 35 GeV/c^2. Clear signals are seen. Also shown is the background from the two photon process. A similar result is obtained from the $\mu^+\mu^-$ channel, although the missing mass resolution is somewhat worse. Ten events in the combined e^+e^- and $\mu^+\mu^-$ channels would constitute a discovery. Table XI summarizes the number of Z^o's needed for 10 detected events as a function of the Higgs mass.

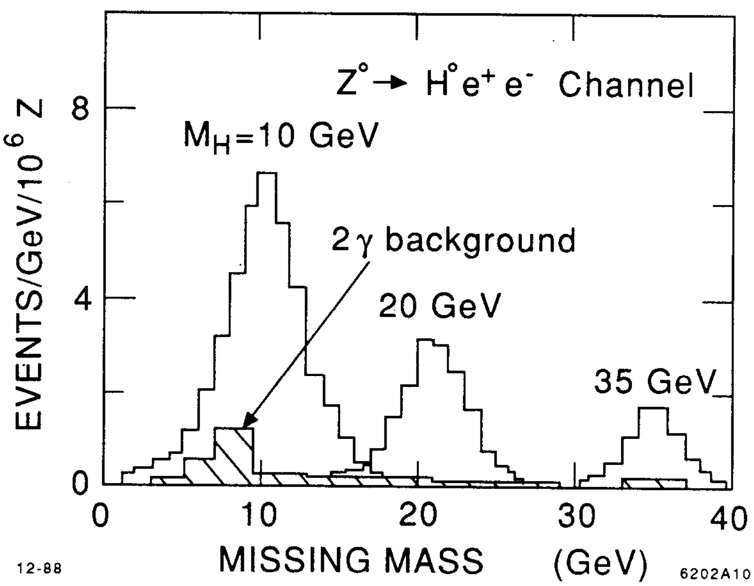

Fig. 33. The Higgs signal from $Z^0 \to H^0e^+e^-$. The expected backgrounds are also shown.

Table XI. The number of Z^o's required to produce 10 detected events as a function of the Higgs mass. The missing mass resolution for the $Z^o \to e^+e^-H^o$ channel is given.

M_{H^o}(GeV)	# Z/10 Events	$\sigma_m(e^+e^-)$ GeV/c^2
4	2×10^4	1.2
10	2×10^5	1.1
25	6×10^5	0.9
35	2×10^6	0.7

Assuming the search was successful and we found a peak in the recoil mass spectrum, how do we know that we have discovered the Higgs scalar? We would have to verify that the signal decayed isotropically and that the couplings favored the heaviest fermion pair available.

We can measure the decay angular distribution as follows. First, we would reconstruct the two-jet directions from the particles associated with the jets. From the ℓ^+ and ℓ^- momenta we can reconstruct $\vec{P}_{H^o}$. Knowing M_{H^o} and $\vec{P}_{H^o}$, we can transform the jet directions into the H^0 center of mass and plot the decay angular distribution. (This method will work as long as we can make the assumption that the decay angular distribution is symmetric about $\theta^* = 90°$. This is because we don't know how to distinguish the jet from the anti-jet (θ^* from $\pi - \theta^*$) and hence by plotting both we are assuming a symmetric decay distribution. Realistically the major problem with this procedure will be the limited statistics. Optimistically one might have ≈ 50 events to play with.

Now, how about measuring if the coupling is proportional to m_f^2? Here the procedure would depend on M_{H^o}. Suppose, as is likely, that $M_{H^o} > 10$ GeV/c^2 in which case $H^0 \to b\bar{b}$ almost exclusively (see Fig. 29). As discussed in Sec. 5.2, using a vertex detector one can expect to tag events containing two b jets with an efficiency $\gtrsim 40\%$, and this with very little contamination from c jets. This can be done because the b quark has a long measured (~ 1 psec) lifetime. So one would subject the $H^0\ell^+\ell^-$ candidate events to this test and if indeed half (= tag efficiency) the events were tagged as having a b jet, one would feel fairly confident that the H^0 decayed predominantly to $b\bar{b}$. If $M_{H^0} < 10$ GeV/c^2 the obvious signal to look for would be $H^0 \to \tau^+\tau^-$.

To summarize the H^0 search then, it is probable that if $M_{H^0} \lesssim 40$ GeV/c^2 it can be found at the Z^0 . We will require a machine with excellent luminosity – $\langle \mathcal{L} \rangle > 10^{30}$ cm^{-2} sec^{-1} to achieve a mass search region of $\lesssim 40$ GeV/c^2. With sufficient statistics ($\gtrsim 50$ events) the H^0 decay angular distribution and coupling can probably be inferred.

9. PHYSICS BEYOND THE MINIMAL STANDARD MODEL

9.1 The Higgs Sector

There is no compelling reason to assume the minimal Higgs scheme with one doublet (four fields); a two doublet scheme as discussed in Sec. 3 is quite permissable. In such a symmetry breaking scheme one has five physical scalars—two neutral scalars H_1^o, H_2^o, one pseudoscalar h^o, and two charged Higgs particles, $H^\pm$. For decay purposes the usual rule applies—couplings are largest for the heaviest fermion decay products permissable.

The search for H_1^o, H_2^o proceeds exactly as descirbed before except that in the non-minimal case the 7.5 GeV/c^2 lower limit on the H^o mass no longer applies. Searching for H^o below 7.5 GeV/c^2 has the advantage of increasing production rate (see Fig. 31). However, for masses below a few GeV/c^2, two-photon backgrounds begin to present a significant problem.

$H^\pm$ are produced in pairs via the reaction $Z^\circ \to H^+H^-$ with a branching fraction $BF(Z^\circ \to H^+H^-) = 1.5\%\ \beta^3$, where β is the velocity to the $H^\pm$. From PETRA experiments, it is known that $M_{H^\pm} > 15$ GeV/c^2 and therefore the dominant decay mode, will be $H^\pm \to b\bar{c}$ ($\approx 75\%$) with the next most favored decay mode being $H^\pm \to \tau^\pm\nu_\tau$. Therefore, most of the events ($\approx 55\%$) coming from $Z^\circ \to H^+H^-$ will be four-jet events. The topologically more attractive modes involving τ's are considerably less probable. Given the relatively small production rate (especially at larger masses) one will most likely focus attention on the four-jet topology. Higher order QCD will produce four-jet events in standard hadronic decays at a rate of $\approx BF(Z^\circ \rightarrow hadrons)\alpha_s^2 \approx 1.5\%$, comparable to the rate of signal events. However, a series of cuts have been developed which provide sufficient suppression of this background, that statistically significant signals can be extracted with $\gtrsim$ 20,000 Z°'s.

The analysis[5d] requires that the events be partitioned into four jets. Using a χ^2 optimization procedure one can chose the best combination of two pairs of jets which fits the hypothesis of pair production of two equal mass objects. The jets are required to be relatively well separated (not true for the majority of QCD four-jet events) and the calculated $H^+(H^-)$ momentum vector is required to point into the well instrumented region of the MARKII. Given the assignment of the jets to the H^+ and H^- hemispheres, an average $H^\pm$ mass can be calculated for each event. The distribution of this mass is shown in Fig. 34 for the background and three different $H^\pm$ mass hypotheses. Ten thousand Z°'s were assumed in the simulation. At the 10,000 Z° event level, indications of the $H^\pm$ signals appear above the background. With 50,000 Z°'s, $H^\pm$ in the mass range from 15 $\rightarrow M_z/2$ GeV/c^2 would not be missed.

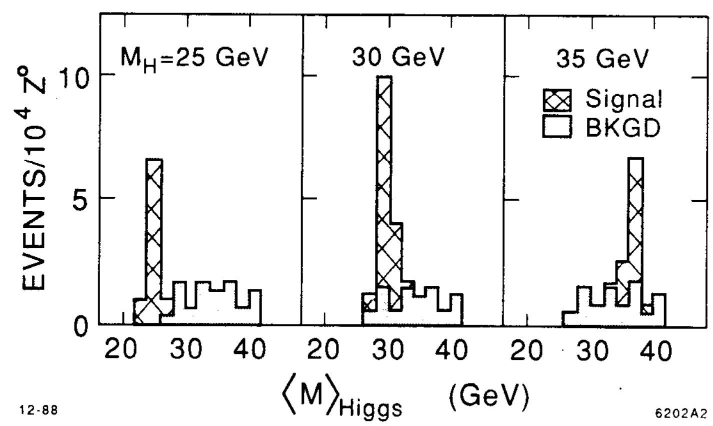

Fig. 34. Dijet invariant mass for the $Z^\circ \rightarrow H^+H^-$ search. The analysis procedure is described in the text.

9.2. Supersymmetry

Supersymmetric theories (SUSY) provide a natural solution to the hierachy problem of the Standard Model by introducing a bosonic (fermionic) partner for every fermionic (bosonic) particle in the Standard Model spectrum. This enlarged fermion and scalar constituent spectrum provides an opportunity to test Nature for the validity of SUSY. SUSY also contains, at a minimum, two Higgs doublets and therefore five physical Higgs particles, as discussed earlier.

Production cross sections for the partners of the normal fermions are characteristic of scalars, namely:

$$R_{\tilde{s}\tilde{\bar{s}}} = \frac{1}{4} R_{f\bar{f}} \quad .$$

Here, $\tilde{s}$ indicates a SUSY scalar whose normal partner is denoted by f. However, there are two SUSY partners for each normal fermion; so in reality

$$R_{\tilde{s}\tilde{\bar{s}}} = \frac{1}{2} R_{f\bar{f}}$$

and

$$\frac{d\sigma_{\tilde{s}\tilde{\bar{s}}}}{d\cos\theta} = \frac{1}{2}\beta^3 \sin^2\theta \sigma_{f\bar{f}} \quad .$$

So, if $M_{\tilde{s}} < M_Z/2$, SUSY scalars could add considerably to the width of the Z^0. As we said previously, if Γ_Z is too wide there could be many reasons for it. One would have to search for each possibility separately.

Scalar leptons with $M_{\tilde{\ell}} < M_z/2$ will be produced at a rate $BF(Z^0 \to \tilde{\ell}^+\tilde{\ell}^-) = 1\frac{1}{2}\%\ \beta^3$ where β is the scalar lepton velocity. Presumably $\tilde{\ell}^\pm \to \ell^\pm\ \tilde{\gamma}$ and, assuming the $\tilde{\gamma}$ is stable, one gets a very distinctive signature—namely events at the Z^0 which have two high energy leptons (e^+e^-, $\mu^+\mu^-$ or $\tau^+\tau^-$) with large missing P_t and energy. The presence of a stable, light particle ($\tilde{\gamma}$) in the decay chains of all the SUSY particles implies that SUSY events are characterized by missing P_t and energy. This is a key element in the search for SUSY signatures.

Backgrounds arise from normal dilepton $(e^+e^-, \mu^+\mu^-, \tau^+\tau^-)$ production, but these are relatively easily eliminated by requiring large missing P_t and energy. The main problem is statistics, the β^3 factor provides an increasing barrier as one probles closer to $M_z/2$. Since the present limit on $M_{\tilde{e}}$ is larger than $M_z/2$, the most sensible channel to search for is $Z^\circ \to \tilde{\mu}^+\tilde{\mu}^-$. For $M_{\tilde{\mu}} = 35$, 40 and 43 Gev/c^2 one produces 41, 18 and 7 $\tilde{\mu}\bar{\tilde{\mu}}$ events respectively per 10^4 Z°; detected events will be half these numbers due to the analysis cuts. There is sensitivity up to the kinematic limit of $M_z/2$ given a data set of $\lesssim$ 50,000 Z°'s; far fewer Z°'s are needed to discover a $\tilde{\mu}$ with a mass of 40 GeV/c^2. Note that $Z^\circ \to \tilde{\tau}^+\tilde{\tau}^-$ can be similarly pursued—the main difference being that the detector efficiencies are somewhat lower.

The story is similar for the scalar quarks where instead of acoplanar two-particle events comprising the signal, acoplanar two-jets are sought. The background comes from standard $Z^\circ \to$ *hadrons* which can be removed with cuts in missing P_t and energy. Background estimates are relatively small, but do depend to some extent on the details of the QCD simulation models. Production rates are relatively large; $BF(Z^\circ \to \tilde{u}\bar{\tilde{u}}) = 6.6\%\ \beta^3$, $BF(Z^\circ \to \tilde{d}\bar{\tilde{d}}) = 5.3\%\ \beta^3$ where β is the quark velocity. The scalar quark will decay to a quark and a gluino or $\tilde{\gamma}$ and hence one has events with two jets which are not back-to-back but have substantial missing P_t and energy. A sample of 20,000 Z°'s is sufficient to cover searches over the full kinematic range.

For scalar neutrinos $BF(Z^0 \to \tilde{\nu}\bar{\tilde{\nu}}) = 3\%\ \beta^3$ where β is the $\tilde{\nu}$ velocity. In order to discuss this channel further requires a decay scheme for the $\tilde{\nu}$. The schemes are complicated by the fact that one has no idea of the scalar electron, scalar $\nu, \ldots$ masses. Certainly a prominent decay mode will be $\tilde{\nu} \to \nu\tilde{\gamma}$, an invisible mode which could have a branching fraction $\simeq 0.6$. There are also multiple charged particle modes possible as shown in Fig. 35 taken from Barnett et al.[13] How much will $Z^0 \to \tilde{\nu}\bar{\tilde{\nu}}$ contribute to the ν counting experiment? The contribution per SUSY species relative to a ν species will be

$$N_{\tilde{\nu}}/N_{\nu} = BF^2(\tilde{\nu} \rightarrow \nu\tilde{\gamma})\,\frac{\Gamma(Z^0 \rightarrow \tilde{\nu}\bar{\tilde{\nu}})}{\Gamma(Z^0 \rightarrow \nu\bar{\nu})} \approx 0.2 \quad ,$$

where I have used $BF(\tilde{\nu} \rightarrow \nu\tilde{\gamma}) \simeq 0.4$. In all likelihood then, it will be hard to see a scalar ν species in the neutrino counting experiment. However, the possibility that scalar neutrinos exist could place systematic limits on how well one would measure N_{ν}.

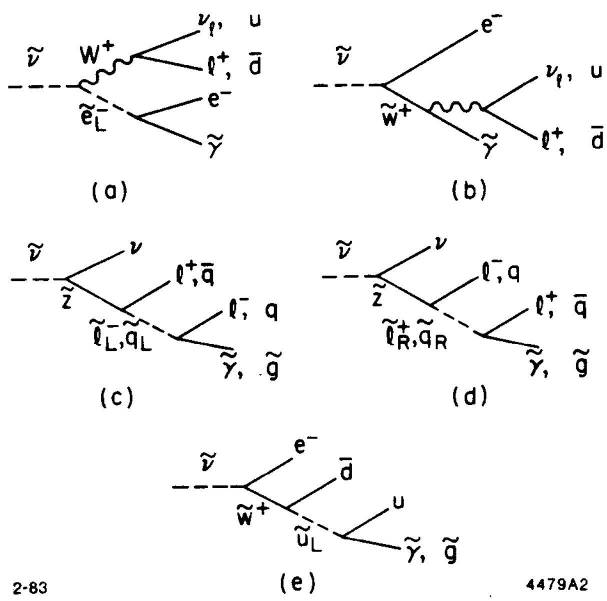

Fig. 35. Possible decay modes for $\tilde{\nu} \rightarrow$ multiple charged particles taken from the model of Barnett et al., Ref. 13.

The multicharge decays shown in Fig. 35 could generate some spectacular events at Z^0. The topology

$$Z^0 \rightarrow \tilde{\nu}\bar{\tilde{\nu}}$$
$$\quad\hookrightarrow \nu\tilde{\gamma}$$
$$\hookrightarrow \nu_e e^- e^+ \tilde{\gamma}$$

would yield an electron and positron in one hemisphere of the detector and nothing else! Even if $BF(\tilde{\nu} \rightarrow \nu_e e^+ e^- \tilde{\gamma}) \approx 10^{-3}$, 10^5 Z^0's would yield ~ 4 such events!

Another interesting topology would be

$$
\begin{array}{l}
Z^0 \to \tilde{\nu}\bar{\tilde{\nu}} \\
\qquad \hookrightarrow \nu\tilde{\gamma} \\
\quad \hookrightarrow e^- q\bar{q}\tilde{g} \quad ,
\end{array}
$$

yielding an electron, two quark jets and a gluino in one hemisphere and nothing visible recoiling against them. The electron energy is expected to be large ($\langle P_e \rangle \approx 8$ GeV) making them easy to detect. Certainly, if SUSY is correct, there is a chance that we could see some spectacular events at the Z^0 .

What about the charginos $\omega^\pm$, $h^\pm$ which are the spin 1/2 partners of the $W^\pm$ and $H^\pm$. Since they couple weakly, these particles look like heavy leptons $L^\pm$ discussed earlier. They decay via

$$
\begin{array}{l}
h^\pm, w^\pm \to W^\pm \tilde{\gamma} \\
\qquad\qquad \hookrightarrow \ell^\pm \nu \text{ or } q\bar{q} \quad .
\end{array}
$$

The decay will be the same as $L^\pm \to W^\pm \nu$ except for effects arising from large $\tilde{\gamma}$ mass. How are they distinguished from $L^\pm$? Consider for the moment the unmixed case for which the weak couplings are

$$
\begin{aligned}
v &= (T_{3L} + T_{3R} - 2Q \sin^2 \theta_w) \\
a &= T_{3L} - T_{3R}
\end{aligned}
$$

with

$$
\begin{aligned}
T_{3L} = T_{3R} &= \pm 1 \qquad \text{for } w^\pm \\
T_{3L} = T_{3R} &= \pm 1/2 \quad \text{for } h^\pm \quad .
\end{aligned}
$$

Hence $v_{w^\pm} = 1.56$, $v_{h^\pm} = 0.56$, and $a_{w^\pm} = a_{h^\pm} = 0$. So, for this unmixed case

$$
\frac{\Gamma(Z^0 \to w^+ w^-)}{\Gamma(Z^0 \to \tau^+ \tau^-)} = 9.6
$$

and

$$
\frac{\Gamma(Z^0 \to h^+ h^-)}{\Gamma(Z^0 \to \tau^+ \tau^-)} = 1.2 \quad .
$$

Hence, charginos could add as much as $\sim 33\%$ to Γ_Z. The search for $w^\pm$, $h^\pm$ proceeds exactly as the search for $L^\pm$ discussed earlier.

How does one distinguish the $L^\pm$ from the $w^\pm$, $h^\pm$? Their weak interactions are very different! The charge asymmetry is

$$\begin{aligned} A_{F-B} &= \frac{3v_e a_e v_f a_f}{(v_e^2 + a_e^2)(v_f^2 + a_f^2)} \\ &= 4.3\% \ \text{ for } L^\pm \ , \\ &= 0 \text{ for } w^\pm,\ h^\pm \text{ in the unmixed case.} \end{aligned}$$

We have considered the simplest unmixed case. Suppose the $w^\pm$ and $h^\pm$ are maximally mixed in states $\tilde{w}_1$ and $\tilde{w}_2$. Then

$$\frac{\Gamma(Z^0 \to \tilde{w}_1^+ \tilde{w}_1^-)}{\Gamma(Z^0 \to \tau^+\tau^-)} = \frac{\Gamma(Z^0 \to \tilde{w}_2^+ \tilde{w}_2^-)}{\Gamma(Z^0 \to \tau^+\tau^-)} = 5.5$$

and

$$A_{F-B}^{\tilde{w}_1} = 14\%$$

$$A_{F-B}^{\tilde{w}_2} = -14\% \quad .$$

Of course, we have no guidance from the theory as to what level of mixing, if any, there is.

10. CONCLUSIONS

I have chosen in these lectures to highlight the more speculative or discovery-oriented measurements because they exemplify the potential of the SLC physics program to make a significant impact on our understanding of Nature. In particular what emerges is the diversity of central issues which can be confronted with a data set as small as 10^4 Z°'s. Many leading questions are probed at this level, the least impressive being the neutral Higgs sector where sensitivity to masses in the 40 GeV/c^2 range require a data set on the order of 10^6 Z°'s. As one moves towards data sets in the 10^5 Z° range, there is the potential to study any new physics which has emerged at the 10^4 level, as well as benefit from what will be very substantial samples of Z° decays to the conventional, known leptons and quarks. Considerable "bread and butter" physics will be possible which will greatly add to our present knowledge of the details of the Standard Model.

In the absence of e^- polarization, very precise tests of the electroweak structure require large ($10^6 Z^\circ$'s) statistics. However, having an electron beam with 45% polarization enhances one's sensitivity by a factor of about 50.

Finally, the Z° is a new frontier and surprises could well be lurking—let's hope so.

11. ACKNOWLEDGMENTS

I wish to thank my hosts at both the St. Croix and Banff schools for their kind invitation and their wonderful hospitality. I also wish to thank the students and fellow lecturers who enriched the lecture experience with their perceptive questions and interesting discussions. I also wish to thank Sharron Lankford and the staff of the SLAC publications department for preparing this document.

REFERENCES

1. (a) *Future Frontier for e^+e^- Collisions: Physics of SLC and LEP*, SLAC–PUB–3928 and *Proceedings of New Frontiers on Particle Physics*, Lake Louise, Canada, February 1986 and (b) *Z° Decay Modes – Experimental Measrement*, SLAC–PUB–3407 and *Proceedings of the 1984 Theoretical Advanced Study Institute on Elementary Particle Physics.*

2. G. Arnison *et al.,* Phys. Lett. **126B**, 398 (1983). (UA1) and P. Bagnaia *et al.,* Phys. Lett. **129B**, 130 (1983) (UA2).

3. For a derivation of this cross section and most of the formulae quoted in this chapter see C. Quigg, *Gauge Theories of the Strong, Weak and Electromagnetic Interactions.*

4. J. Alexander *et al.,* Phys. Rev. D **37**, 56 (1988).

5. (a) CERN Yellow Reports 76–18 (1976) and 79–01 (1979). (b) Proceedings of the SLC Workshop on Experimental use of the SLC; SLAC–247 (1982). (c) Proceedings of the Cornell Z° Theory Workshop; CLNS 81–485. (d) Proceedings of the 2nd and 3rd MARKII Workshop on SLC Physics, SLAC–REPORT–306, and SLAC–REPORT–315.

6. U. Amaldi *et al.,* Phys. Rev. D **36**, 1385 (1987).

7. R. N. Cahn, Phys. Rev. D **36**, 2666 (1987).

8. W. Marciano *et al.,* Phys. Rev. D **29**, 1810 (1984).

9. J. Kuhn *et al.,* Nucl. Phys. B **272**, 560 (1986).

10. G. Wormser, SLAC–PUB–3509.

11. J. D. Bjorken, SLAC–198 (1976).

12. J. Finjord, Physica Scripta, Vol. **21**, 143 (1980).

13. R. M. Barnett et al., Phys. Rev. D **29**, 1990 (1984).